A STUDY ON EHD FLOW INDUCED BY RECTIFIED IONS

AYAKO YANO

SEPTEMBER 2017

A STUDY ON EHD FLOW INDUCED BY RECTIFIED IONS

A dissertation submitted to
THE GRADUATE SCHOOL OF ENGINEERING SCIENCE
OSAKA UNIVERSITY
in partial fulfillment of the requirements for the degree of
DOCTOR OF PHILOSOPHY IN ENGINEERING

BY

AYAKO YANO

SEPTEMBER 2017

Abstract

In the previous research, electrohydrodynamic (EHD) flow was known as an electrically driven flow with discharge in liquids. However, conventional methods require at least several tens of volts of applied voltage to make electrically polarized conditions. In this thesis, a novel method is proposed to generate an ion-drag EHD flow by applying relatively low voltages.

Firstly, a flow channel was designed to rectify ion transport pathways using an anion exchange membrane in which a small pore was made for the channel. An EHD flow dragged by the cation transport on the order of 1 mm/s was observed by applying 2.2 V in a 0.1 mol/L NaOH aqueous solution. The flow showed a transient response, which was visualized by tracking polystyrene particles dispersed in the solution as a tracer. That is, velocity response rapidly rose up and gradually decayed to zero. The responses of voltage difference along the flow direction were also measured by probe electrodes inserted into the solution at both ends of the channel with a distance of 3 mm. When voltage is applied to the bias electrodes, the response of voltage difference showed a peak and soon decayed to the constant value. When using the membrane with a small pore, the peak voltage showed the maximum value. This result indicated that our device effectively concentrated cations in the flow channel to generate the EHD flow.

Secondly, a constant current of 0.8 mA was applied to induce an EHD flow in the same condition described above. In this case, transient responses of the EHD flow were observed, which was similar trend to the results of constant voltage applications. It was confirmed that ionic currents, which were rectified by the anion exchange membrane with the flow channel, caused to drive the liquid flow, where electroneutrality was locally broken.

Thirdly, we investigated the dependence of generated EHD flows on the concentration. NaOH aqueous solutions of 1.0×10^{-1}, 1.0×10^{-2} and 1.0×10^{-3} mol/L were used for the experiments. The values of peak velocity increased as the concentration. On the other hand, when using a solution of 1.0×10^{-3}mol/L NaOH, any significant EHD flow was not observed. Visualizing the flows in the channel, it was found that the velocity profile appeared to be a Poiseuille flow that was driven by constant pressure. This result elucidated that the observed flows is obviously different from plug like electroosmotic

flows typically observed in micro- and nanochannels.

Finally, it was concluded that EHD flow was successfully developed in aqueous solutions by using an ion exchange membrane with a flow channel. When a cation transport pathway was constrained in the channel, solvent molecules strongly dragged by the cations and developed a EHD flow. Using this method, the applied voltage value was drastically decreased and it enabled us to use it in aqueous solutions avoiding the instability of water electrolysis. Furthermore, this finding is expected to shed light on the frontier of micro- and nanofluidic technologies.

Contents

1 General Introduction **1**

1.1 Background 1

1.2 Electrohydrodynamic flow 2

1.3 Liquid flows in micro- and nanoscales 2

1.4 Aims and structure of this thesis 3

2 Electrohydrodynamic Flow through a 1-mm^2 Cross-Section Pore Placed in an Ion-Exchange Membrane **6**

2.1 Introduction 7

2.2 Theoretical Model of an EHD Flow though a Pore 9

2.3 Experimental Methods 14

2.4 Results and Discussion 15

2.4.1 Theoretical analysis of EHD flow through a pore in ion-exchange membranes 15

2.4.2 Visualization and electrical observation of EHD flow 21

2.4.3 EHD flow to sequential applications of electric potentials 25

2.5 Conclusion 30

3 Observation of Electrohydrodynamic Flow through a Pore in Ion-Exchange Membrane **34**

3.1 Introduction 35

3.2 Experimental Methodology 38

3.2.1 Design of experimental device 38

3.2.2 Experimental method 38

3.3 Results and Discussion 39

3.3.1 Confirmation of the experimental condition 39

3.3.2 Anion-exchange membrane 39

3.3.3 EHD generation by applying constant voltages 42

3.3.4 Effects of membrane treatments on electric current 42

3.4 Conclusion 45

4 Concentration Dependence of Cation-Induced Electrohydrodynamic Flow Passing Through an Anion Exchange Membrane 48

4.1 Introduction 49

4.2 Experimental Methodology 52

4.3 Results and Discussion 55

4.3.1 Experimental observations 55

4.3.2 Numerical analysis of cation-induced EHD flow 62

4.4 Concluding Remarks 69

5 General Conclusion 76

Chapter 1

General Introduction

1.1 Background

Recently, increases of world wide problems about energy consumption, environmental pollution and the rapid provision of medical technology in crisis are worried about. Researches using micro- and nanofluidic devices fabricated by micro-electro-mechanical systems (MEMS) have attracted significant attention because of the capability of various applications for the problems mentioned above. Many researchers reported fundamental studies about micropumps [2, 3, 4] and micromixing devices [7]. Such microfluidic devices have expected to be applied for various research fields. For example, a blood test which could be examined by a small amount of liquids. It has been extensively studied. The base sequencing technology of deoxyribonucleic acid (DNA) and ribonucleic acid (RNA) have also been one of the hottest topics, where single molecule identification at high speed with high accuracy was achieved [25, 6, 7]. These devices succeeded to sense tiny changes in ionic current by finely tuning the signal-to-noise ratio. A single molecule passing through a nanopore could be identified more quickly than the conventional methods that used enzyme reactions and electrophoresis in agarose gel. However, there remains a lot of problems, where ionic current also has to be controlled to introduce DNA and RNA molecules into a nanopore. Many theoretical models of ionic current in electrolyte solutions have been proposed. Electric forces are preferably applied for a driving force to induced a liquid flow, where wall surfaces are dominantly exposed to the liquid compared with the volume in microfluidic channels. Such a electrically driving method receives

much attention because of its simple mechanism and possibility of downsizing.

1.2 Electrohydrodynamic flow

Liquid flows driven by electric forces are known as electrohydrodynamic (EHD) flows [19, 13, 14, 15]. To drive EHD flows, excessively high voltages had to be applied to directly inject electrical charges into liquids. That is, electric discharges were required to occur in liquids. Therefore, a variety of oils was usually employed for a good candidate of solvents, because oils were usually more stable in high voltages than water that theoretically electrolyzes at 1.23 V of the applied voltage. Recently, electro-conjugate fluids have been investigated for engineering and medical applications. On the other hand, EHD flows have never been effectively available in aqueous solutions, although detailed flow control methods have been required. There is a difficulty to apply electric body forces in liquids, because positive and negative ions usually attract each other via Coulomb interactions, maintaining electroneutrality. Rectification of transport pathways of cation and anion is important to realize electrically polarized conditions. In this study, we examine an idea to generate an EHD flow in electrically polarized condition in relatively low voltages, although conventional methods required at least tens of volts of the applied voltage.

1.3 Liquid flows in micro- and nanoscales

On the other hand, when a channel surface in electrolyte solution is electrically charged, counterions interact with the surface charges and form a highly concentrated boundary layer which is called electric double layer (EDL). In conventional ion transport theories, an EDL thickness is assumed to be much smaller than the cross-section of a channel, where electroneutrality is maintained everywhere except for very near the walls. However, phenomena that could not be explained by the conventional models were often observed in micro- and nanochannels [28]. When the channel width is reduced to the same order of thickness of EDL, the electroneutrality is broken in the channel. An electroosmotic flow (EOF) is driven by the transport of concentrated counterions in EDLs when an electric pontenial is applied. Especially in nanochannels, EDLs of opposite channel sur-

faces overlap with each other and then, the velocity profile is similar to a Poiseuille flow. In the case of microchannel, the velocity profile becomes plug like flow because of the slip boundary of EDLs [25, 28, 24]. Applied voltages to drive a liquid flow can be reduced by downsizing the flow channels. Nanochannels [36] can reduce the applied voltage lower than microchannels [26, 1], although the flow rate also becomes lower.

1.4 Aims and structure of this thesis

As introduced above, in this study, we perform experiments to generate EHD flows in aqueous solutions by using an anion exchange membrane and a pore in the membrane to reduce the applied electric potential. In Chapter 2, an novel method to rectify the transport pathways of both cation and anion is supposed and in such a condition, an externally applied electric potential drives an EHD flow, where tracer particles are tracked to visualize flow fields. Herein, a NaOH aqueous solution is employed for the working liquid that is separated into two parts by an anion exchange membrane. Constant electric potentials are applied in the aqueous solutions. In Chapter 3, based on the fundamental principle, constant electric current conditions are also examined to generate EHD flows, using the same methods and the same device in the former chapter. The importance of rectified ionic currents is discussed. In Chapter 4, the dependency of ion concentrations on the EHD flow is investigated. The flow velocity, flow rate, and duration time are suspected to be related with the ion concentrations. The ionic current and electric potential difference are measured by probes placed at both ends of the flow channel. Finally, in Chapter 5, the results obtained in this thesis are summarized with perspectives in the future work.

Bibliography

[1] A. Brask, G. Goranović, M. J. Jensen, and H. Bruus. A novel electro-osmotic pump design for nonconducting liquids: theoretical analysis of flow rate–pressure characteristics and stability. *J. Micromech. Microeng.*, 15(4):883, 2005.

[2] Y. S. Kim, J. H. Kim, K. H. Na, and K. Rhee. Experimental and numerical studies on the performance of a polydimethylsiloxane valveless micropump. *Proc. Inst. Mech. Eng. C: J. Mech. Eng. Sci.*, 219(10):1139–1145, 2005.

[3] K.-S. Yun, I.-J. Cho, J.-U. Bu, C.-J. Kim, and E. Yoon. A surface-tension driven micropump for low-voltage and low-power operations. *J. Microelectromech. Sys.*, 11(5):454–461, 2002.

[4] A. O. El Moctar, N. Aubry, and J. Batton. Electro-hydrodynamic micro-fluidic mixer. *Lab Chip*, 3(4):273–280, 2003.

[5] H. Daiguji, P. Yang, and A. Majumdar. Ion transport in nanofluidic channels. *Nano Lett.*, 4(1):137–142, 2004.

[6] James Clarke, Hai-Chen Wu, Lakmal Jayasinghe, Alpesh Patel, Stuart Reid, and Hagan Bayley. Continuous base identification for single-molecule nanopore dna sequencing. *Nature nanotechnology*, 4(4):265–270, 2009.

[7] Stefan W Kowalczyk, Maarten W Tuijtel, Serge P Donkers, and Cees Dekker. Unraveling single-stranded dna in a solid-state nanopore. *Nano letters*, 10(4):1414–1420, 2010.

[8] J. R. Melcher and G. I. Taylor. Electrohydrodynamics: A review of the role of interfacial shear stresses. *Annu. Rev. Fluid. Mech.*, 1:111–146, 1969.

[9] D. A. Saville. Electrohydrodynamics: The taylor–melcher leaky dielectric model. *Annu. Rev. Fluid. Mech.*, 29:27–64, 1997.

[10] W. D. Ristenpart, I. A. Aksay, and D. A. Saville. Assembly of colloidal aggregates by electrohydrodynamic flow: Kinetic experiments and scaling analysis. *Phys. Rev. E*, 69:021405–1–021405–8, 2004.

[11] W. D. Ristenpart, I. A. Aksay, and D. A. Saville. Electrohydrodynamic flow around a colloidal particle near an electrode with an oscillating potential. *J. Fluid. Mech.*, 575:83–109, 2007.

[12] R. B. Schoch, J. Han, and P. Renaud. Transport phenomena in nanofluidics. *Rev. Mod. Phys.*, 80:839–883, 2008.

[13] D. Ross, T. J. Johnson, and L. E. Locascio. Imaging of electroosmotic flow in plastic microchannels. *Anal. Chem.*, 73(11):2509–2515, 2001.

[14] Y. Takamura, H. Onoda, H. Inokuchi, S. Adachi, A. Oki, and Y. Horiike. Low-voltage electroosmosis pump for stand-alone microfluidics devices. *Electrophoresis*, 24(1-2):185–192, 2003.

[15] S.-S. Hsieh, H.-C. Lin, and C.-Y. Lin. Electroosmotic flow velocity measurements in a square microchannel. *Colloid Polym. Sci.*, 284(11):1275–1286, 2006.

[16] S. Zeng, C.-H. Chen, J. C. Mikkelsen, and J. G. Santiago. Fabrication and characterization of electroosmotic micropumps. *Sens. Actuat. B*, 79(2):107–114, 2001.

Chapter 2

Electrohydrodynamic Flow through a 1-mm^2 Cross-Section Pore Placed in an Ion-Exchange Membrane

Abstract

In recent years, the control of ionic currents has come to be recognized as one of the most important issues related to the efficient transport of single molecules and microparticles in aqueous solutions. However, the complicated liquid flows that are usually induced by applying electric potentials have made it difficult to address a number of unsolved problems in this area. In particular, the non-equilibrium phenomena that occur in electrically non-neutral fields must be more thoroughly understood. Herein, we report on the development of a theoretical model of liquid flows resulting from ion interactions while focusing on the so-called electrohydrodynamic (EHD) flow. We also discuss the development of an experimental system to optically and electrically observe EHD flows using a 1 mm^2 cross-section pore placed in an ion-exchange membrane where cation and anion flows can be separated without the use of a charged environment. Although micro/nano-sized flow channels are usually applied to induce electric double layer overlaps in order to utilize strong electroosmotic effects, our system does not require such laborious fabrication processes. Instead, we visualize EHD flows by using a millimeter size pore immersed in an alkaline aqueous solution. In this setup, liquid flows passing through the

pore along the direction of ion flow, whose velocity reaches on the order of 1 mm/s, can be clearly observed by applying a few volts of electric potential. Furthermore, the transient phenomena associated with ionic responses are theoretically elucidated.

Keywords

Electrohydrodynamic flow, Ion transport, Visualization, Ion-exchange membrane

2.1 Introduction

In recent decades, the use of micro/nanofluidic devices in the creation of novel bionanotechnologies has attracted significant attention. As a result, a number of cutting-edge devices such as the electrochemical capacitor, [1, 2, 3, 4, 5] the ion electric field transistor, [25, 7, 8, 1, 23] and the single molecule sequencer, [11, 12, 9, 14, 15, 16, 10, 18] have been developed. In these technologies, the behavior of electrolyte ions plays an important role in improving output efficiencies. In an aqueous solution, electrolyte ions are exposed to externally applied fields. In particular, ions or electrically charged particles are driven by the electric force known as electrophoresis, [19, 28, 29, 46] and liquid flows induced by surface charges on a wall are known as electroosmotic flow (EOF). [28, 29, 32, 24] In micro/nanofluidic devices, electrolyte solutions are strongly polarized in an electric double layer (EDL) near a channel wall, which cause EOF parallel to the wall surface. To induce strong flow fields, finely tuned conditions are satisfied, such as ensuring that the facing walls are less than a few tens of nanometers apart, and that salt concentrations are kept less than 1 mM [28, 29]. In conventional models, it is believed that positive and negative ions are usually paired. Therefore, such solutions are considered to be electrically neutral everywhere except near the electrically charged surfaces [25]. More specifically, oppositely signed ions are usually equilibrated in solution because even a modest elongation of an equilibrium length between two ions results in a strong Coulomb force that causes them to attract each other. Accordingly, focusing on microscopic confined spaces, further understanding will be necessary for future progress.

Electrohydrodynamics was first explored in the pioneering works of Melcher and Tay-

lor [19] and Saville [13]. Additionally, an assembly of polystyrene particles enhanced by electrohydrodynamic (EHD) flows was experimentally observed by Trau et al. [28, 14] and numerically analyzed by Ristenpart et al. [15]. Furthermore, EHD micropumping applications [31, 20] and EHD flow variations [33, 34] were reported in some literatures. Essentially, EHD flows are based on external electric force applied to liquid flows, where an electric potential expressed by the Poisson equation plays an external force in the Navier–Stokes equation. In actual systems, EHD flow observations are only possible in highly polarized conditions such as those shown in EDL [28, 14, 20] and in the strong electric fields required to apply at least several tens of volts of electric potential [31, 20]. EOF is particularly effective on flows near EDL and is, therefore, often combined with EHD. This means that it is difficult to detect EOF separately from electrically charged surfaces in bulk solutions due to the electroneutrality factor, as mentioned above. [25]

Because we are also interested in ion transports in various spatial scales, [27, 36, 15, 46] in this study, we investigate EHD flows in aqueous solutions, while proposing a novel method that does not require any difficult fabrication processes. Specifically, a 1 mm^2 cross-section pore is made in an ion-exchange membrane that has a cross-sectional area large enough to negate the effect of surface charges. Then, water flow driven by ionic motions is observed by using a microscope and a high-speed camera. Using this experimental system, it is possible to use the membrane pore to separate the current paths of negative and positive ions. Short-duration non-equilibrium responses just after applying an electric potential can be detected by applying a few volts of electric potential in an aqueous solution corresponding to an electric field on the order of 100 V/m. It should be noted that highly tuned techniques and time-consuming processes are not needed to prepare such a device. After the response, the liquid flow seems to equilibrate to a steady current condition. This finding means that an electrically polarized condition can be induced at a area far from the electrode surfaces. That is, the breakdown of electroneutrality in bulk solutions is achieved. Furthermore, the time and spatial scales of the phenomenon can be well explained by a theoretical EHD flow model.

2.2 Theoretical Model of an EHD Flow though a Pore

In this section, we show the development of a theoretical model for EHD flow through ion-exchange membranes. First, incompressible liquid flow, which is driven by electric fields, is expressed by the Navier–Stokes equations:

$$\rho_m \left(\frac{\partial}{\partial t} + \mathbf{u} \cdot \nabla \right) \mathbf{u} = -\nabla p + \mu \triangle \mathbf{u} + \sum_i \rho_i \mathbf{E}, \tag{2-1}$$

$$\nabla \cdot \mathbf{u} = 0, \tag{2-2}$$

where ρ_m is the mass density, $\mathbf{u}(\mathbf{r},t)$ is the velocity, μ is the viscosity, $p(\mathbf{r},t)$ is the pressure, $\mathbf{E}(\mathbf{r},t)$ is the electric field, and $\rho_i(\mathbf{r},t)$ is the electric charge density of the ith species. In electrolyte solutions, ion behavior is described by the Nernst–Planck equation:

$$\frac{\partial \rho_i}{\partial t} = -\nabla \cdot \mathbf{j}_i, \tag{2-3}$$

$$\mathbf{j}_i = \left(\frac{z_i e \mathbf{E}}{\zeta_i} - D_i \nabla + \mathbf{u} \right) \rho_i, \tag{2-4}$$

where z_i is the valence number, e is the elementary charge, ζ_i is the friction coefficient, and D_i is the diffusion coefficient. The electric fields and electric current density obey the Maxwell equations:

$$\varepsilon \varepsilon_0 \nabla \cdot \mathbf{E} = \sum_i \rho_i, \tag{2-5}$$

$$\mathbf{j} = \sum_i \mathbf{j}_i + \varepsilon \varepsilon_0 \frac{\partial \mathbf{E}}{\partial t}, \tag{2-6}$$

$$\nabla \cdot \mathbf{j} = 0, \tag{2-7}$$

where ε and ε_0 are the relative dielectric constant and dielectric constant of vacuum. By substituting eqs 2-5 and 2-6 into eq 2-7, eqs 2-3 and 2-4 are found to be satisfied. That is, ionic currents in electrolyte solutions satisfy the Maxwell equations. When variables are non-dimensionalized as follows:

$$\mathbf{r}^* = \frac{\mathbf{r}}{L}, \quad \mathbf{u}^* = \frac{\mathbf{u}}{U}, \quad t^* = \frac{Ut}{L}, \quad \rho_i^* = \frac{L\rho_i}{\varepsilon_0 E_0}, \quad \mathbf{j}_i^* = \frac{\mathbf{j}_i L^2}{\varepsilon_0 E_0 D_i}, \quad \mathbf{E}^* = \frac{\mathbf{E}}{E_0}, \quad p^* = \frac{p}{\rho_m U^2}, \tag{2-8}$$

where L is the characteristic length, U is the characteristic velocity, and E_0 is the uniform electric field, eqs 2-1 and 2-2 are transformed to

$$\left(\frac{\partial}{\partial t^*} + \mathbf{u}^* \cdot \nabla\right)\mathbf{u}^* = -\nabla p^* + \frac{1}{\mathrm{Re}}\triangle \mathbf{u}^* + \xi \sum_i \rho_i^* \mathbf{E}^*, \tag{2-9}$$

$$\nabla \cdot \mathbf{u}^* = 0, \tag{2-10}$$

where $\xi = \varepsilon_0 E_0^2/(\rho_m U^2)$ and Re is the Reynolds number. Equations 2-3 and 2-4 become

$$\frac{\partial \rho_i^*}{\partial t^*} = -\frac{1}{\alpha_i \mathrm{Pé}} \nabla \cdot \mathbf{j}_i^*, \tag{2-11}$$

$$\mathbf{j}_i^* = \left(\eta_i^* \mathbf{E}^* - \nabla + \alpha_i \mathrm{Pé} \mathbf{u}^*\right) \rho_i^*, \tag{2-12}$$

where we focus on a diffusion coefficient D_m of mainly effective species and set to $\alpha_i = D_m/D_i$ and then, the Péclet number is defined as $\mathrm{Pé} = LU/D_m$. Additionally, the non-dimensionalized mobility is defined as $\eta_i^* = z_i e E_0 L/\zeta_i D_i$. Furthermore, eqs 2-5–2-7 result in

$$\varepsilon \nabla \cdot \mathbf{E}^* = \sum_i \rho_i^*, \tag{2-13}$$

$$\mathbf{j}^* = \sum_i \frac{1}{\alpha_i \mathrm{Pé}} \mathbf{j}_i^* + \varepsilon \frac{\partial \mathbf{E}^*}{\partial t^*}, \tag{2-14}$$

$$\nabla \cdot \mathbf{j}^* = 0. \tag{2-15}$$

Hereafter, we will omit the asterisk symbol for non-dimensionalization. According to the schematic illustration in Figure 2-1, we assume that the velocity field is dominant along the pore axis (z-axis) such that $\mathbf{u} = (0, 0, u_z)$. The velocity field is constant along the z-axis, and thus u_z is independent of z such that $u_z = u_z(x, y, t)$, where $(x, y) \in [0, 1] \times [0, 1]$ for a square cross-section and $t \in [0, \infty)$. As mentioned above, the driving force of the liquid depends on the charge difference of electrolyte ions within a short period, as described by eqs 2-11 and 2-12, where the ionic current response consists of electrophoresis, diffusion, and convection. The relationship between the electric charge density and electric field is given by the Poisson equation (eq 2-13), and thus the electric field depends on ion behavior.

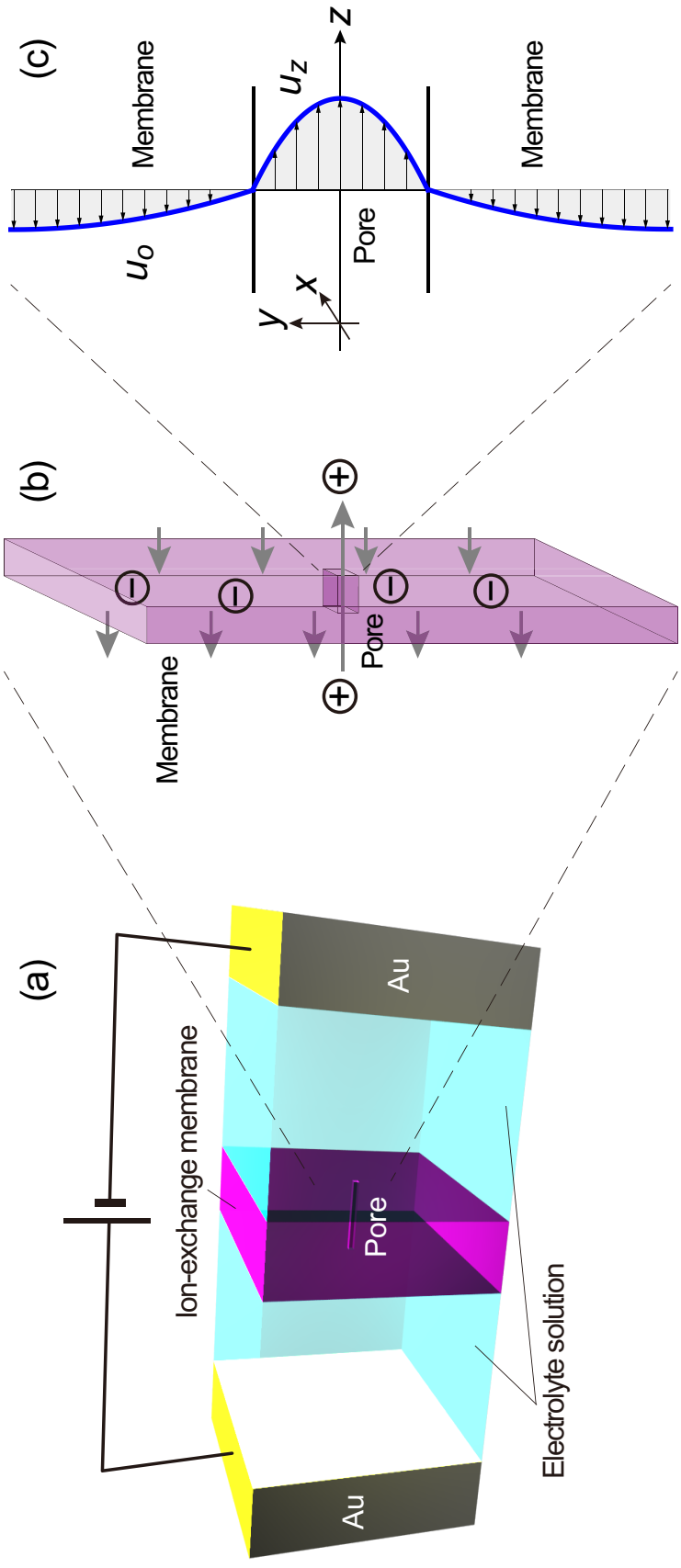

Figure 2-1. Schematic illustrations of theoretical model. (a) An ion-exchange membrane in which a small pore is placed is immersed in an electrolyte solution and then exposed to external electric fields. (b) When an anion-exchange membrane is immersed in an alkaline solution, anions can pass through the entire face, whereas cation penetration is limited to the pore. (c) In such ion transport situations, EHD flows will be induced separately in both the membrane and pore.

According to the numerical results of the coupled Nernst–Planck and Poisson equations provided in a previous study [46], the non-uniformity of electric fields is apparent near electrodes, and weak uniform fields remain in solution at points farther away from the electrodes. In our experimental setup, the flow channel is sufficiently separated from both electrodes to allow the electric fields in the pore to be potentially approximated as uniform along the z-axis. Associated with the numerical solution, we replace the non-dimensionalized electric force in eq 2-9 by

$$\sum_i \rho_i(z,t)E(z,t) \equiv \rho(z,t)E(z,t) \approx \sum_j f_j \exp\left(-\lambda_j t\right). \tag{2-16}$$

The force field is represented by exponents with the amplitude f_j and time scale λ_j, where these constants are determined from experimental results. As usual, it is known that the EHD flows are proportional to the square of the electric field strengths [20]. In our model, the electric force is also proportional to E_0^2 insofar as $\sum_i \rho_i$ and E are uniform in eq 2-9. On the other hand, in actual systems, concentrations and electric fields tend to deviate from uniformity very near the electrodes causing them to screen the surface charges. When the upper surface of the liquid is fully exposed to air and the pressure gradient is assured to be negligibly small compared to the electric force term, eqs 2-9 and 2-10 are replaced by

$$\frac{\partial u_z}{\partial t} = \frac{1}{\mathrm{Re}}\triangle u_z + \xi \sum_j f_j \exp\left(-\lambda_j t\right) \quad \text{in pore,} \tag{2-17}$$

$$\frac{\partial u_o}{\partial t} = \frac{1}{\mathrm{Re}}\triangle u_o + \xi \sum_j f'_j \exp\left(-\lambda'_j t\right) \quad \text{in ion}-\text{exchange membrane,} \tag{2-18}$$

where Re is assumed to be the same in both regions. Due to the continuity of liquid flow, eqs 2-17 and 2-18 should satisfy

$$\int_S u_z \mathrm{d}x\mathrm{d}y + \int_{S'} u_o \mathrm{d}x\mathrm{d}y = 0. \tag{2-19}$$

For non-slip boundary conditions in the pore and an initial condition:

$$u_z(0,y,t) = u_z(1,y,t) = 0, \tag{2-20}$$

$$u_z(x,0,t) = u_z(x,1,t) = 0, \tag{2-21}$$

$$u_z(x,y,0) = 0, \tag{2-22}$$

solving eq 2-17, we obtain

$$u_z(x,y,t) = -\frac{16\xi}{\pi^2}\sum_{n_x}\sum_{n_y}\sum_{i}\frac{f_i}{n_x n_y}\frac{\exp(-\lambda_i t)-\exp(-\lambda_k t)}{\lambda_i-\lambda_k}\sin k_x x \sin k_y y, \tag{2-23}$$

$$k_x = n_x\pi,\ \ n_x = 1,3,5,\cdots, \tag{2-24}$$

$$k_y = n_y\pi,\ \ n_y = 1,3,5,\cdots, \tag{2-25}$$

$$\lambda_k = \frac{(n_x^2+n_y^2)\pi^2}{\mathrm{Re}}. \tag{2-26}$$

In the ion-exchange membrane, the reverse flow of counterions is effectively developed in $(x,y)\in[0,l']\times[0,l']$. For initial and boundary conditions:

$$u_o(0,y,t) = u_o(l',y,t) = 0, \tag{2-27}$$

$$u_o(x,0,t) = u_o(x,l',t) = 0, \tag{2-28}$$

$$u_o(x,y,0) = 0, \tag{2-29}$$

we obtain

$$u_o(x,y,t) = -\frac{16\xi}{\pi^2}\sum_{n_x}\sum_{n_y}\sum_{i}\frac{f_i'}{n_x n_y}\frac{\exp\left(-\lambda_i' t\right)-\exp\left(-\lambda_k' t\right)}{\lambda_i'-\lambda_k'}\sin k_x' x \sin k_y' y, \tag{2-30}$$

$$k_x' = \frac{n_x\pi}{l'},\ \ n_x = 1,3,5,\cdots, \tag{2-31}$$

$$k_y' = \frac{n_y\pi}{l'},\ \ n_y = 1,3,5,\cdots, \tag{2-32}$$

$$\lambda_k' = \frac{(n_x^2+n_y^2)\pi^2}{\mathrm{Re}\,l'^2}. \tag{2-33}$$

Furthermore, to satisfy eq 2-19, a relation between f_i and f_i' results in

$$\frac{\sum_{n_x}\sum_{n_y}\sum_i f_i' n_x^{-2} n_y^{-2}\left(\lambda_i'-\lambda_k'\right)^{-1}\left[\exp\left(-\lambda_i' t\right)-\exp\left(-\lambda_k' t\right)\right]}{\sum_{n_x}\sum_{n_y}\sum_i f_i n_x^{-2} n_y^{-2}(\lambda_i-\lambda_k)^{-1}\left[\exp(-\lambda_i t)-\exp(-\lambda_k t)\right]} = -\frac{1}{l'^2}. \tag{2-34}$$

2.3 Experimental Methods

Figure 2-2 shows schematic illustrations of our experimental setup, in which an ion-exchange membrane with a 1 mm^2 cross-section pore is immersed in a 0.1 M NaOH aqueous solution. Helical-shaped Au electrodes are placed on both sides of the membrane and set at a distance at least 5 mm from each other (Figures 2-2a,b). To facilitate OH^- and anion exchange, an anion-exchange membrane (NEOSEPTA®, ASTOM Co., Ltd., Tokyo, Japan) is employed. The membrane is about 140 μm thick. The reservoir, which holds different-sized cylindrical chambers, is made of polydimethylsiloxane (PDMS). The cylinder with the anion-exchange membrane fixed at one end is 14.4 mm in diameter and 5 mm in length. Another chamber (18.4 mm in diameter and 15 mm in length) is set outside the one mentioned above into which a glass cylinder (18.0 mm in diameter and 10 mm in length) and a spacer (18.0 mm in diameter and 5 mm in length) are placed, as shown in Figure 2-2a. A 1×1 mm^2 cross-section pore penetrates 3 mm into the PDMS channel and is placed in the anion-exchange membrane. Here, we chose a square cross-section to ensure high tracer particle contrast to transmitted light. The surface area of the ion-exchange membrane immersed in the solution is at least 100 times larger than that of the pore. A 0.8 μm sized polystyrene particle (Estapor®, MERCK KGaA Co., Ltd., Dermstadt, Germany) is employed as a tracer, where 10 volume percent of the polystyrene particles is further diluted to 0.1 volume percent, and 200 μL of it is diffused in 3.6 mL of the NaOH solution. Before measurements, the electrodes are electrically shorted, the solutions are stirred, and left for more than 20 min. After that, the equilibrium condition is confirmed by observing the behavior of tracer particles. When an electric potential is applied to the Au electrodes, the motions of tracer particles are observed using a microscope equipped with a high-speed camera (VW–9000, Keyence Co., Ltd., Osaka, Japan) (Figure 2-2c). The applied potential difference is absolutely set to 2.2 V in order to obtain clear electric signals. The measurements are carried out at a constant voltage condition. Motions of the particles are tracked with the high-speed camera at a frame rate of 500 fps. Trajectories are traced and their velocity is analyzed. Electric signals are simultaneously measured with a sampling rate of 200 Hz by using a potentiostat (VersaSTAT4, AMTEK, Inc., TN, USA).

2.4 Results and Discussion

2.4.1 Theoretical analysis of EHD flow through a pore in ion-exchange membranes

In this section, we first discuss a case of a single exponential electric signal decay caused by ionic responses. Since ionic response differences are not locally distinguished in the actual system, it is reasonable to set an equivalent response time, $\tau_e = \lambda_e^{-1}$, in the pore and ion-exchange membrane. Thus, eq 2-34 is expressed as

$$\frac{f_e'}{f_e} = -\frac{1}{l'^2}\frac{\sum_{n_x}\sum_{n_y} n_x^{-2} n_y^{-2}(\lambda_e - \lambda_k)^{-1}[\exp(-\lambda_e t) - \exp(-\lambda_k t)]}{\sum_{n_x}\sum_{n_y} n_x^{-2} n_y^{-2}\left(\lambda_e - \lambda_k'\right)^{-1}\left[\exp(-\lambda_e t) - \exp\left(-\lambda_k' t\right)\right]}, \tag{2-35}$$

where the amplitude of the electric signal corresponds to f_e and f_e' for the inside and outside of the pore, respectively. Hereafter, we will discuss the case of $f_e = 1$. Figure 2-3 shows u_z, u_o, and f_e' analyzed for varieties of λ_e and l' at Re = 0.1, where the velocity evaluated at the center of channel, $x = y = 0.5$, is presented and is normalized by ξ. As shown in Figure 2-3a, we found that a u_z response strongly depends on λ_e when we set $l' = 1.414$. The liquid response time tends to increase with decreasing λ_e. The relative difference between the time scales of liquid flow and the electric signal affects the result. Due to the continuity of the volume flow rate, the velocity is significantly lower in the ion-exchange membrane than in the pore, as far as $l' > 1$. Figure 2-3b presents the magnitude of f_e' as a function of time. According to eq 2-35, f_e' rapidly settles at some steady state values and converges to l'^{-4} as λ_e decreases. Notably, f_e' deviates from the convergence value as λ_e is close to λ_k and λ_k'. Figures 2-3c,d show results for the case of $l' = 3.162$. The flow velocity in the ion-exchange membrane is apparently reduced in comparison with Figure 2-3a, since the cross-sectional area of the flow channel increases proportionally to l'^2. The asymptotic behavior of f_e' is qualitatively the same as Figure 2-3b, although there is a quantitative difference associated with l'^{-4}. Figure 2-4 shows results for the case of Re = 1. An increase in Re reduces both λ_k and λ_k' and results in

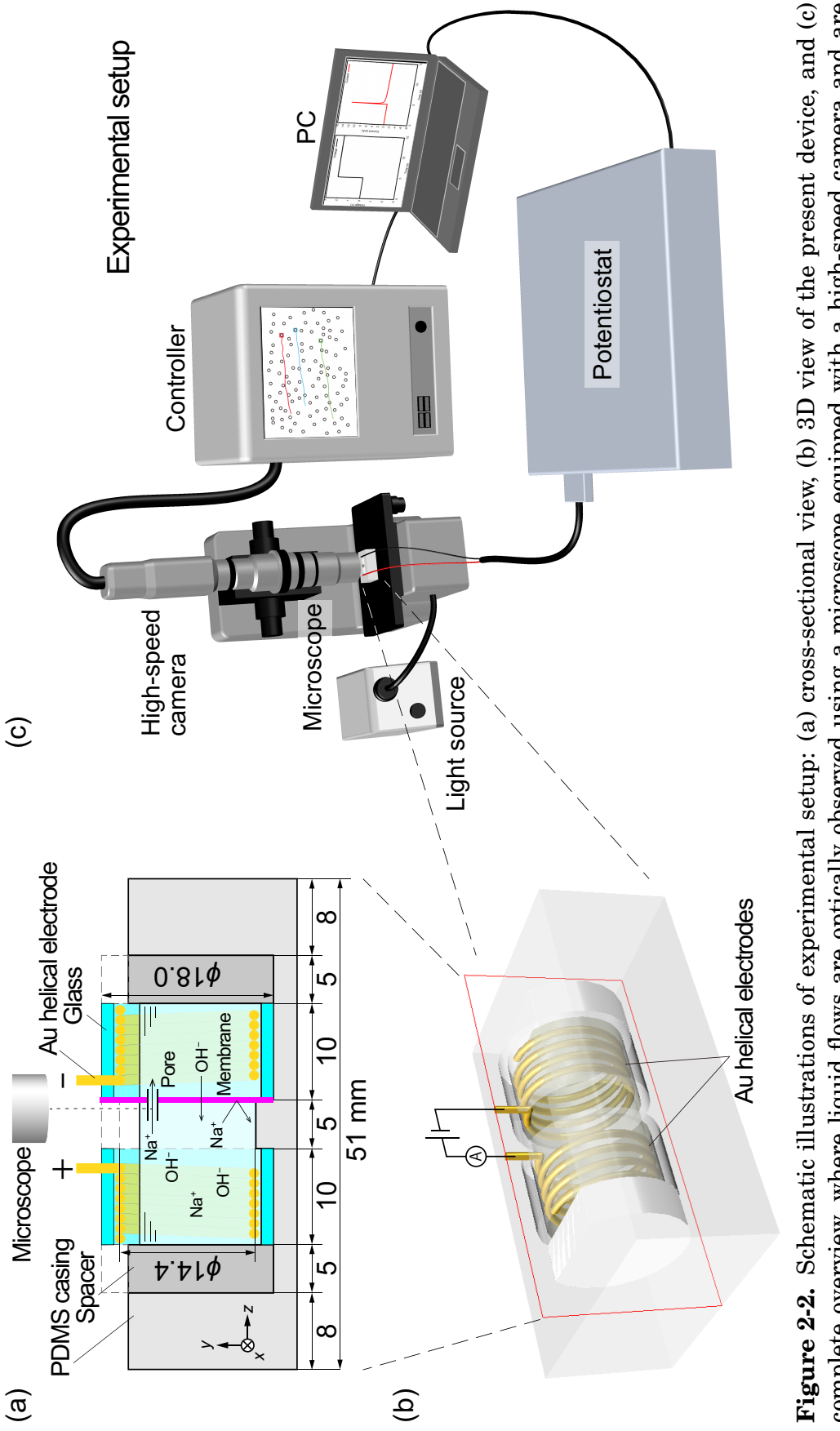

Figure 2-2. Schematic illustrations of experimental setup: (a) cross-sectional view, (b) 3D view of the present device, and (c) complete overview, where liquid flows are optically observed using a microscope equipped with a high-speed camera and are electrically measured using a potentiostat.

the slow liquid flow response. As shown in Figure 2-4a, the initial rise of u_z and u_o takes slightly more time, even though the decay of flow velocities is similar to that in Figure 2-3. Some maximum peaks can be found in the transient responses. Additionally, the behavior of f_e' is different from that in Figure 2-3b. In particular, as shown in Figure 2-4b, f_e' tends to approach zero when $\lambda_e = 10$. In the case of $l' = 3.162$, u_z and u_o exhibit similar trends with Figure 2-4a, except for the small amplitude of u_o, as shown in Figure 2-4c. On the other hand, f_e' tends to deviate from l'^{-4} when $\lambda_e > 1$ and, in particular, approaches zero (Figure 2-4d). Figure 2-5 presents results from the case of Re = 10. Initial increases and subsequent decays in the transient responses are clearly found in Figure 2-5a. In Figure 2-5b, the response of f_e' also becomes slower and approaches zero when $\lambda_e > 1$. As shown in Figures 2-5c,d, an increase in l' reduces u_o and f_e' is clearly modulated by relative differences between λ_e, λ_k, and λ_k'. Based on the difference in the surface areas, it is clear that u_z and f_e become prominent compared to u_o and f_e', respectively. It has been suggested that the flow field can be magnified relatively in the pore when we design $l' \gg 1$ in actual experimental systems. Figure 2-6 shows velocity profiles as a function of time along the x-axis at $y = 0.5$ for the case of $\lambda_e = 1$ and $l' = 1.414$. As shown in Figures 2-6a,b, for small Re, the velocity field develops quickly and decays as a Poiseuille flow. As Re increases in the manner shown in Figure 2-6c, where the development of velocity fields can be detected, the liquid flow develops almost uniformly during the initial rise and gradually deforms to a Poiseuille flow.

In this section, we discussed an EHD flow that could be realized using a small pore in ion-exchange membranes. It was theoretically demonstrated that temporal EHD flows can be generated if electroneutrality is eliminated by applying electric potentials in electrolyte solutions. Furthermore, it is possible to induce liquid flows associated with the charge difference of ions and electric fields in the pore. As a result, we clarified that the time scale of ionic responses and Re govern the behavior of liquid flows. In the following subsection, we show an experiment performed to confirm that the electroneutrality is actually broken, which then induces an EHD flow.

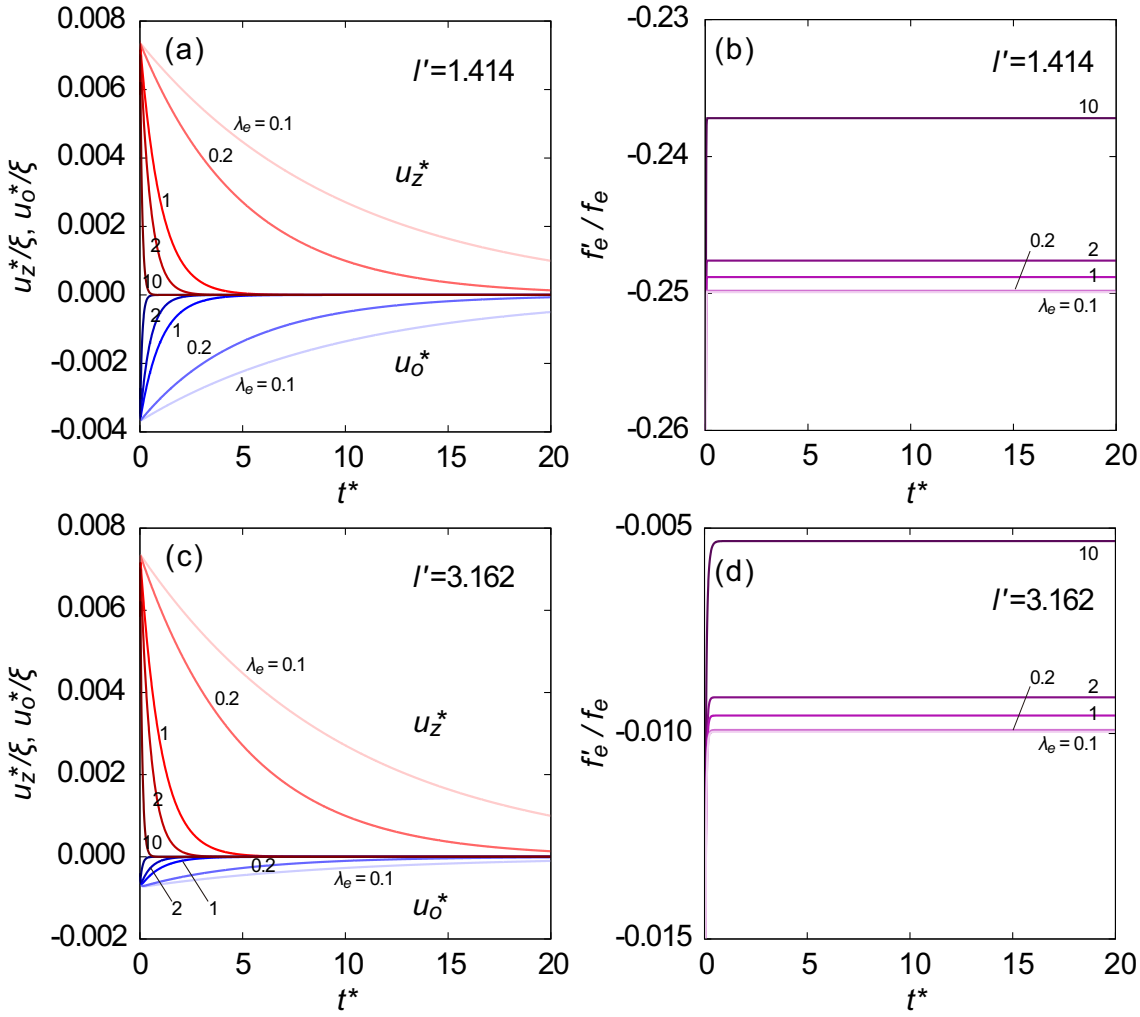

Figure 2-3. Numerical results of the theoretical model for Re = 0.1: (a) normalized u_z and u_o and (b) f_e'/f_e for $l' = 1.414$; (c) u_z and u_o and (d) f_e'/f_e for $l' = 3.162$. λ_e is varied ranging from 0.1 to 10. u_z and u_o calculated at $(x, y) = (0.5, 0.5)$ are presented.

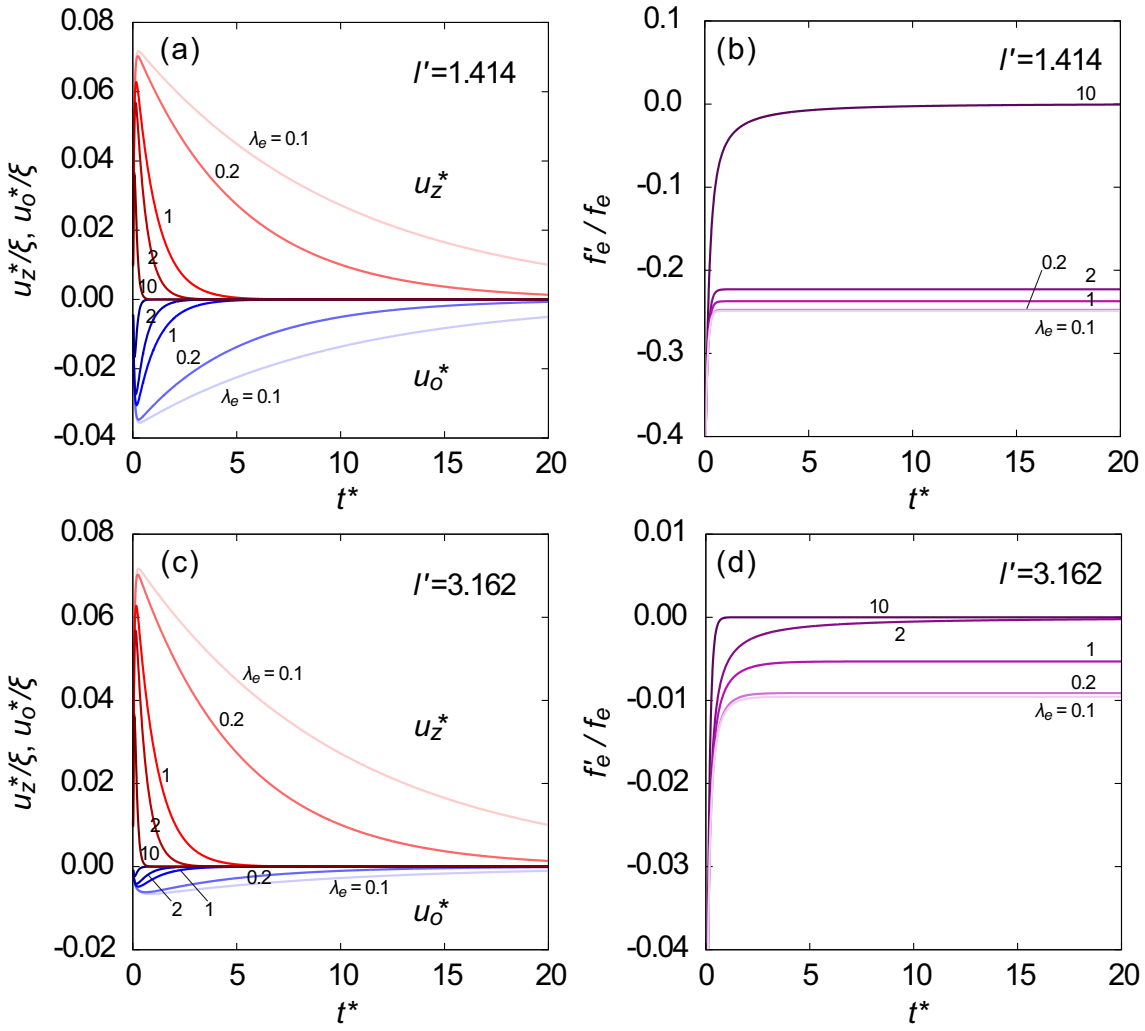

Figure 2-4. Numerical results of the theoretical model for Re = 1: (a) normalized u_z and u_o and (b) f_e'/f_e for $l' = 1.414$; (c) u_z and u_o and (d) f_e'/f_e for $l' = 3.162$. λ_e is varied ranging from 0.1 to 10. u_z and u_o calculated at $(x, y) = (0.5, 0.5)$ are presented.

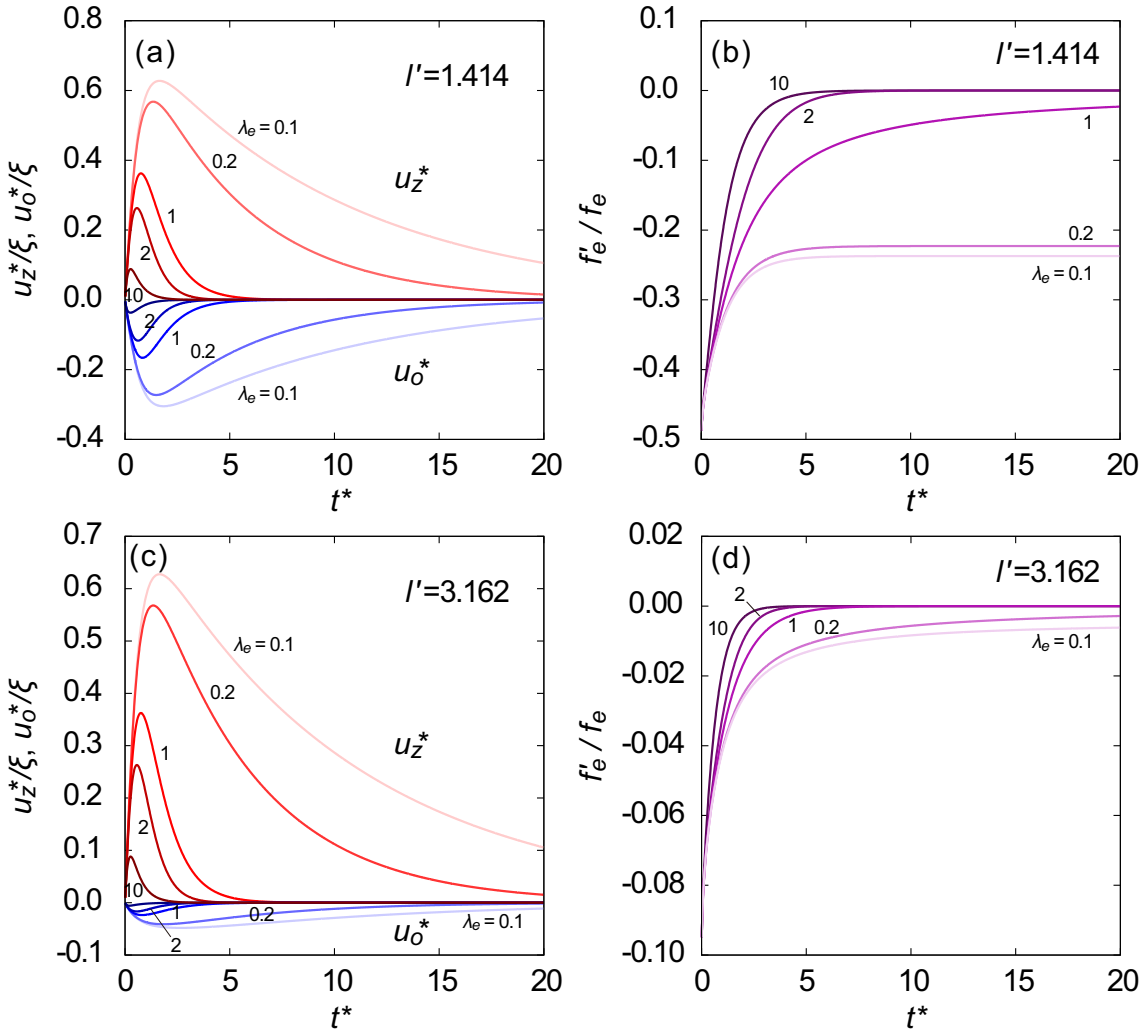

Figure 2-5. Numerical results of the theoretical model for Re = 10: (a) normalized u_z and u_o and (b) f_e'/f_e for $l' = 1.414$; (c) u_z and u_o and (d) f_e'/f_e for $l' = 3.162$. λ_e is varied ranging from 0.1 to 10. u_z and u_o calculated at $(x, y) = (0.5, 0.5)$ are presented.

2.4.2 Visualization and electrical observation of EHD flow

Figure 2-7 shows current-voltage (IV) characteristics of an anion-exchange membrane with and without a pore. In the present experimental system, the conductance of 0.1 M NaOH solution was electrically measured and resulted in 0.25 mS (Figure 2-7a). In this solution, the conductance of the pristine membrane was 0.17 mS (Figure 2-7b) and that of the membrane with a 1×1 mm^2 cross-section pore was 0.12 mS (Figure 2-7c). It was found that the anion-exchange membrane actually became resistant to ionic currents, and that the presence of the pore could not restore equivalent conductance levels. The cross-section area of the PDMS block surrounding the pore possibly blocked the ionic current.

Figure 2-8 shows electric potential responses that were measured by applying a voltage difference of 2.2 V on the helical-shaped bias electrodes, where the other probe electrodes were set across the membrane with the distance of 3mm between the electrodes. Compared between the transient responses with and without a membrane, a prominent peak was observed by using the membrane with a 1×1 mm^2 pore (Figure 2-8(c)). It was found that drastic Na^+ concentration changes transiently occurred near the pore immediately after the electric potential was applied, even though this polarization was not maintained at steady states as shown in Figure 2-7. This trend was also confirmed for the other applied voltages (figures are omitted).

Figure 2-9 shows some typical transient responses of the liquid flow resulting from the trajectories of tracer particles in the area of 458×611 μm^2 ($x \times z$) at the center of the pore, which were independently measured. These results imply that highly concentrated ions in the pore region induce the liquid flow triggered by an applied electric potential. In our experimental system, it was confirmed that electrophoretic transport of the polystyrene particle was not clearly observed in pure water and the NaOH solution, even though the polystyrene particle surfaces were known to have weak negative charges. This means that the electric field strength is too weak to induce electrophoretic particle transport in the bulk condition. Furthermore, in unsteady flows, taking into account the additional mass and Basset force, as well as the Stokes drag, particle response time τ_p is approxi-

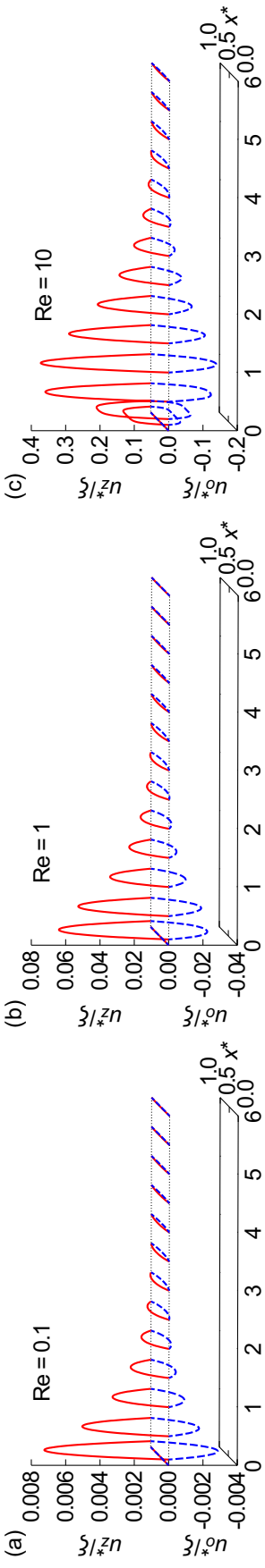

Figure 2-6. Time evolutions of u_z (solid line) and u_o (dashed line) along the x-axis at $y = 0.5$ for (a) Re = 0.1, (b) Re = 1, and (c) Re =10, where $\lambda_e = 1$ and $l' = 1.414$.

mately expressed as [38, 39, 40]

$$\tau_p = \frac{2}{9}\left(\frac{\rho_p}{\rho_m} + \frac{1}{2}\right)\frac{a^2}{\nu}, \tag{2-36}$$

where ρ_p and a are the density and radius of a particle, respectively. In the present case, τ_p is on the order of 1 μs, resulting from $\rho_p/\rho_m \sim 1$, $a \sim 1$ μm, and $\nu \sim 1 \times 10^{-6}$ m^2/s. Such a short response time means that the behavior of particles is fully susceptible to the liquid flow. Actually, the particles simultaneously move in a one-dimensional direction along the z-axis when an electric potential is externally applied. In Figure 2-9a, an electric potential of 2.2 V was externally applied at $t = 5$ s, and electric current signal caused by ionic responses was observed immediately thereafter. Following that, liquid flow rate increased and velocity slowly decreased, even though multiple-spike signals seemed to be included in the decay. At the peak point, the liquid flow velocity reached 1 mm/s. Figure 2-9b also shows a sharp apparent velocity peak, which reached approximately 1.5 mm/s. In this case, the liquid flow response time is shorter than that in Figure 2-9a. In contrast, Figure 2-9c showed liquid response retardation, and severe velocity changes were found when the electric current approached a steady condition. Additionally, some peaks could be found in the liquid response. In each case, the particle transport direction was from the positive to negative electrode, which was also the cation flow direction. Furthermore, peculiar oscillations often appeared by applying electric potentials, which was clearly different from the Brownian motion of particles. This phenomenon has not been theoretically explained. Consequently, it is clear that the liquid flow velocity is strongly enhanced by ionic motions in the solution that is recognized via electric signals, even though there are response variations. These experimental results indicate the observation of EHD flow using this system.

At the maximum velocity of the peaks was found to reach approximately 1 mm/s. Here, assuming a uniform electric field between the two electrodes, the electric field strength is roughly estimated as ~ 100 V/m, which can be evaluated from Figure 2-8. The liquid velocity field is developed by applying an electric potential and shows continuous decay to zero. Furthermore, even though the electric current signal spike can only be observed for a short period, the liquid flow actually occurs during the following

ionic responses. It is, therefore, suspected that an applied electric potential induces ion transport in the electric field, after which a liquid flow is induced in the pore by densely concentrated cations. Although it is believed that ions are usually paired to maintain the electroneutrality of electrolyte solutions, except for externally charged conditions such as EDL at charged surfaces, [25, 28] our results indicate that electroneutrality can be broken without requiring any specific conditions. In our experimental system, the pore was located more than 1 mm away from the electrode. When a pore with a 1 mm^2 square cross-section is filled with water and we apply $L = 1$ mm and $\nu = 1 \times 10^{-6}$ m^2/s, the time constant of the liquid response is evaluated as $\tau = \lambda^{-1} \approx 0.05$ s from eq 2-26. This constant appears to be smaller than that of ionic responses measured by electric signals shown in Figure 2-9. Ionic responses are usually caused by transitions of both ion distributions and electric potentials. Basically, it is a nonlinear response and cannot be determined by a single exponent. This point has already been discussed in a previous study. [46]

As shown in Figure 2-10a, a measured electric signal was fitted by linear combinations of some exponents considering the time constants of $\tau_e = 0.01$, 0.1, 1, and 10 s. Using these constants, experimental data could be fitted by

$$I(t) = 0.0030 \exp\left(-\frac{t}{0.01}\right) + 0.0097 \exp\left(-\frac{t}{0.1}\right) + 0.0010 \exp(-t) + 0.0001 \exp\left(-\frac{t}{10}\right). \quad (2\text{-}37)$$

In this case, the time constant coefficient of 0.1 s resulted in 0.0097 mA, which was the largest. Additionally, the coefficients of 0.01 and 1 s were also included as factors of 0.003 and 0.001 mA, respectively, and I was sufficiently converged at $\tau_e = 10$ s. Assuming that the ionic current obeys Ohm's law, eq 2-37 can be related to electric force in eq 2-23 such that $I = \beta \rho E$, where β is a constant. To represent the experimental data, we set $\beta = 2 \times 10^{-4}$ m^4/Vs. Then, ρ is on the order of 1 Cm^{-3} for $I = 10$ mA, which corresponds to the concentration of 1×10^{-8} M for monovalent ions. The results indicate that the charge separation of ions is very weak in actual systems, even if the concentration of NaOH aqueous solution is 0.1 M in equilibrium, which is why electrolyte solutions are usually considered to be close to electroneutral throughout. [25] According to this experimental data fit, the external force can be applied in eq 2-23, after which the time evolution of u_z produces the results as shown in Figure 2-10b. These results show that firing an electric

spike signal excites the liquid flow and that the successive u_z then shows a maximum peak that slowly decays to zero. Although the contribution of the time constant of 0.1 s may be dominant in eq 2-37, the response of u_z shows a long tail affected by the other time constants. As shown in Figures 2-3–2-5, no single component can explain the characteristics caused by both fast and slow ion responses. That is, ionic responses include various time constants and the EHD flows are driven as expressed in the theoretical model.

2.4.3 EHD flow to sequential applications of electric potentials

Figure 2-11 shows a velocity response resulting from a sequential application of electric potentials and its theoretical model. When an electric potential of 2.2 V was applied at $t = 5$ s and -2.2 V was successively applied at $t = 15$ s, continuous liquid flow responses were clearly observed, as shown in Figure 2-11a. In the same manner as reported in the previous section, the liquid flow velocity first increased, and then showed a slow decay. Furthermore, it also responded to the inversely applied electric potential, and it was found that the EHD flow direction could be reversed sequentially by changing the direction of the electric fields. The mechanism of this phenomenon can be understood using the same model mentioned above. For sequential applications of electric potentials, eq 2-17 is modified as follows

$$\left[\frac{\partial}{\partial t} - \frac{1}{\mathrm{Re}}\triangle\right] u_z = \xi \sum_i \sum_j f_{ij} \exp\left[-\lambda_i (t - t_j)\right] \Theta(t - t_j), \tag{2-38}$$

where $\Theta(t)$ is the step function. In this case, the solution is

$$\begin{aligned} u_z(x,y,t) \;=\; & -\frac{16\xi}{\pi^2} \sum_{n_x} \sum_{n_y} \sum_i \sum_j \frac{f_{ij}}{n_x n_y} \frac{\exp\left[-\lambda_i (t - t_j)\right] - \exp\left[-\lambda_k (t - t_j)\right]}{\lambda_i - \lambda_k} \Theta(t - t_j) \\ & \times \sin k_x x \sin k_y y. \end{aligned} \tag{2-39}$$

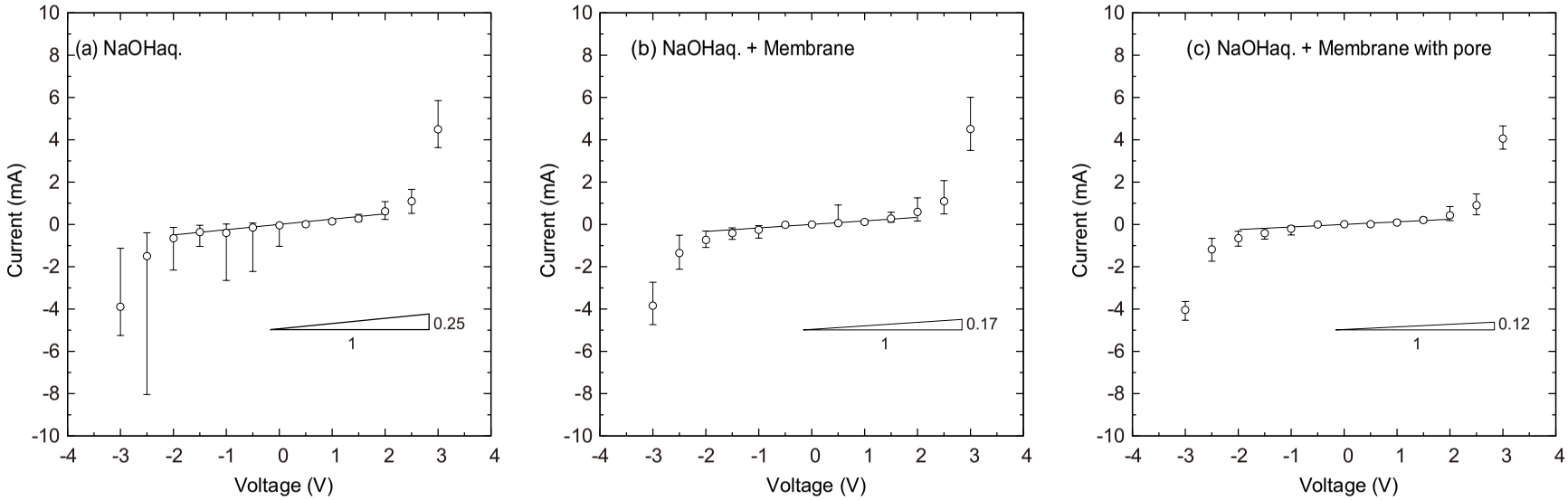

Figure 2-7. *IV* characteristics measured in the present device for the case of (a) 0.1 M NaOH aqueous solution, (b) a pristine anion-exchange membrane in the NaOH solution, and (c) an anion-exchange membrane with 1×1 mm^2 cross-section pore in the NaOH solution. Error bars indicate minimum and maximum values at each data point, resulting from 8 samples in (a) and (b) and 6 samples in (c). The conductance is evaluated by linear least-square fit between -2 and 2 V and results in (a) 0.25 mS, (b) 0.17 mS, and (c) 0.12 mS.

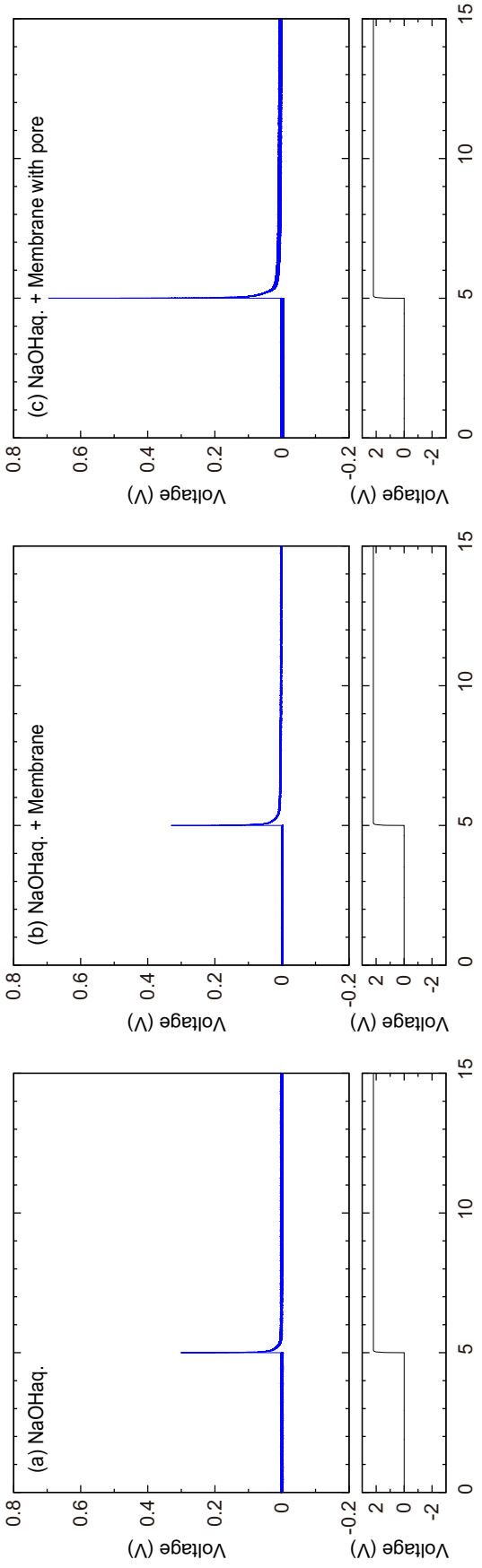

Figure 2-8. Electric potential response between the both ends of membrane when an electric voltage difference of 2.2 V was applied on the helical-shaped bias electrodes in 0.1 M NaOH solution. The other probe was set with the electrode distance of 3 mm (a) without a membrane, (b) across a pristine anion-exchange membrane, and (c) across an anion-exchange membrane with a 1×1 mm^2 cross-section pore.

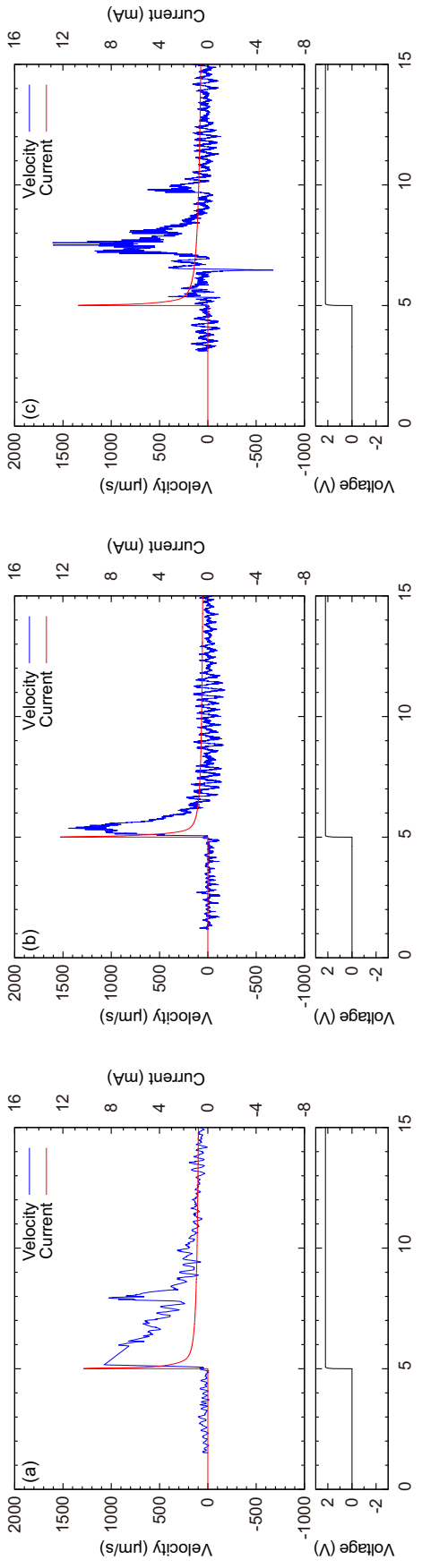

Figure 2-9. Three typical experimental data of the velocity of liquid flow in the pore and electric current, corresponding to the applied electric potential of 2.2 V at $t = 5$ s. (a) Following the quick response of electric current, velocity seems to be multiply firing in the decay process. (b) A sharp single spike of the velocity is observed just following the electric signal. (c) After the application of electric potential, an interval of a few seconds occurs until liquid flow is enhanced. Tracer particles were tracked in the area of 458 × 611 μm^2 ($x \times z$) at the center of the pore.

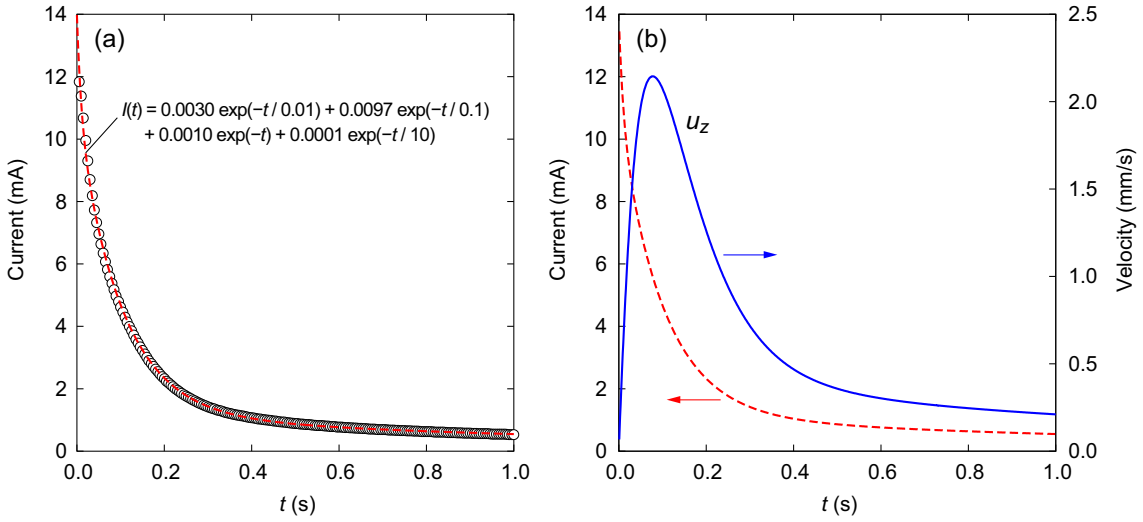

Figure 2-10. (a) Experimental data (open circle) of electric current response and the least-square fit (dashed line) by the set of time constants: 0.01, 0.1, 1, and 10 s. (b) Response of u_z (solid line) at $x = y = 0.5$ induced by the electric current response (dashed line) analyzed in (a), where the electric current is translated to the electric force by $I = \beta\rho E$ and $\beta = 2 \times 10^{-4}$ m^4/Vs.

This result is presented in Figure 2-11b. Here, we employed the same parameter sets used in Figure 2-10. Our theoretical model well explains the response trends in the experimental result, where ionic motions enhance liquid flows. More specifically, the inversely applied potentials disturb the steady current state and induce the backward flow of ionic currents. Then, the cation flow concentrates at the pore and produces the reverse flow. In the experimental result, the magnitude of the second peak of both the current and the velocity is always larger than the first. The results also show that the environments can be changed slightly for successive electric field applications. When compared to the initial equilibrium condition, the possibility exists that there are differences in the Na^+ concentration on either sides subject to the applied potential. Such differences have not yet been taken into account in the theoretical model. Therefore, the present model does not consider the spatial distribution of ions along the electric fields, although the diffusion of ions along the electric fields takes long periods of time. [46] In this study, we could identify such important points by coupling the electric measurement with optical microscopic observation. To facilitate further improvements, coupling the ion transport processes to the growth process of flow fields should be considered.

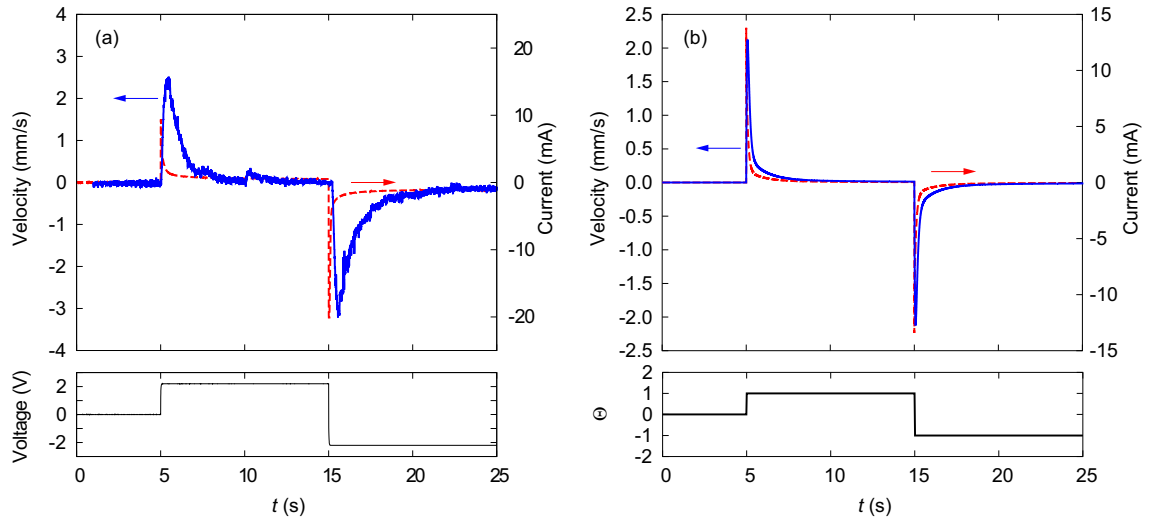

Figure 2-11. (a) Experimental observation and (b) numerical result of the velocity response (upper panels) to sequential applications of electric potential (lower panels), where the flow velocity and electric current are presented with solid and dashed lines, respectively. The first application of electric potential was at $t = 5$ s and the second one was inversely at $t = 15$ s. In the theoretical model shown in (b), the parameter set employed in Figure 2-10 was applied.

2.5 Conclusion

We succeeded in visualizing an EHD flow induced by a cation flow passing through a 1 mm^2 cross-section pore in an anion-exchange membrane while applying an electric potential of 2.2 V on a 10 mm order length system. Contrary to conventional theories, we found that ion flows could be transiently separated using an EHD flow without applying a charge. In our experimental mechanism, the charge difference was induced due to a pore placed in the membrane by applying electric fields, after which a liquid flow on the order of 1 mm/s was observed until electroneutral conditions were reestablished. We also found that the liquid flow response time scale was affected by ion behavior. Furthermore, it was demonstrated that the liquid flow direction could be changed sequentially via the use of inversely applied electric fields. This observation was also well understood using a theoretical model in which even a small charge difference will cause a strong one-dimensional flow. Considering various ion-exchange membrane and electrolyte solution combinations, this kind of EHD flow is expected have applications in mass transport, rectification, and liquid flow mixing.

Bibliography

[1] B. E. Conway. Transition from "supercapacitor" to "battery" behavior in electrochemical energy storage. *J. Electrochem. Soc.*, 138:1539–1548, 1991.

[2] P. Simon and Y. Gogotsi. Materials for electrochemical capacitors. *Nat. Mater.*, 7:845–854, 2008.

[3] D. Wei, M. R. J. Scherer, C. Bower, P. Andrew, T. Ryhänen, and U. Steiner. A nanostructured electrochromic supercapacitor. *Nano Lett.*, 12:1857–1862, 2012.

[4] Z. Xu, Z. Li, C. M. B. Holt, X. Tan, H. Wang, B. S. Amirkhiz, T. Stephenson, and D. Mitlin. Electrochemical supercapacitor electrodes from sponge-like graphene nanoarchitectures with ultrahigh power density. *Phys. Chem. Lett.*, 3:2928–2933, 2012.

[5] H.-C. Han, C.-W. Chong, S.-B. Wang, D. Heh, C.-A. Tseng, Y.-F. Huang, S. Chattopadhyay, K.-H. Chen, C.-F. Lin, J.-H. Lee, and et al. High k nanophase zinc oxide on biomimetic silicon nanotip array as supercapacitors. *Nano Lett.*, 13:1422–1428, 2013.

[6] H. Daiguji, P. Yang, and A. Majumdar. Ion transport in nanofluidic channels. *Nano Lett.*, 4(1):137–142, 2004.

[7] I. Vlassiouk and Z. S. Siwy. Nanofluidic diode. *Nano Lett.*, 7(3):552–556, 2007.

[8] S.-W. Nam, M. J. Rooks, K.-B. Kim, and S. M. Rossnagel. Ionic field effect transistors with sub-10 nm multiple nanopores. *Nano Lett.*, 9(5):2044–2048, 2009.

[9] W. Guan, R. Fan, and M. A. Reed. Field-effect reconfigurable nanofluidic ionic diodes. *Nat. Commun.*, 2:506:1–8, 2011.

[10] W. Guan and M. A. Reed. Electric field modulation of the membrane potential in solid-state ion channels. *Nano Lett.*, 12:6441–6447, 2012.

[11] A. J. Storm, C. Storm, J. Chen, H. Zandbergen, J.-F. Joanny, and C. Dekker. Fast DNA translocation through a solid-state nanopore. *Nano Lett.*, 5(7):1193–1197, 2005.

[12] D. Fologea, J. Uplinger, B. Thomas, D. S. McNabb, and J. Li. Slowing DNA translocation in a solid-state nanopore. *Nano Lett.*, 5(9):1734–1737, 2005.

[13] C. Dekker. Solid-state nanopores. *Nat. Nanotechnol.*, 2:209–215, 2007.

[14] M. Zwolak and M. Di Ventra. Colloquium: Physical approaches to DNA sequencing and detection. *Rev. Mod. Phys.*, 80(1):141–165, 2008.

[15] D. Branton, D. W. Deamer, A. Marziali, H. Bayley, S. A. Benner, T. Butler, M. Di Ventra, S. Garaj, A. Hibbs, X. Huang, and et al. The potential and challenges of nanopore sequencing. *Nat. Biotechnol.*, 26(10):1146–1153, 2008.

[16] M. Tsutsui, M. Taniguchi, K. Yokota, and T. Kawai. Identifying single nucleotides by tunnelling current. *Nat. Naotechnol.*, 5:286–290, 2010.

[17] B. M. Venkatesan and R. Bashir. Nanopore sensors for nucleic acid analysis. *Nat. Nanotechnol.*, 6:615–624, 2011.

[18] T. Ohshiro, K. Matsubara, M. Tsutsui, M. Furuhashi, M. Taniguchi, and T. Kawai. Single-molecule electrical random resequencing of DNA and RNA. *Sci. Rep.*, 2:501:1–7, 2012.

[19] T. Sokalski, P. Lingenfelter, and A. Lewenstam. Numerical solution of the coupled nernst–planck and poisson equations for liquid junction and ion selective membrane potentials. *J. Phys. Chem. B*, 107:2443–2452, 2003.

[20] R. B. Schoch, J. Han, and P. Renaud. Transport phenomena in nanofluidics. *Rev. Mod. Phys.*, 80:839–883, 2008.

[21] W. Sparreboom, A. van den Berg, and J. C. T. Eijkel. Principles and applications of nanofluidic transport. *Nat. Nanotechnol.*, 4:713–720, 2009.

[22] K. Doi, M. Tsutsui, T. Ohshiro, C.-C. Chien, M. Zwolak, M. Taniguchi, T. Kawai, S. Kawano, and M. Di Ventra. Nonequilibrium ionic response of biased mechanically controllable break junction (MCBJ) electrodes. *J. Phys. Chem. C*, 118:3758–3765, 2014.

[23] B. Zhang, Y. Ai, J. Liu, S. W. Joo, and S. Qian. Polarization effect of a dielectric membrane on the ionic current rectification in a conical nanopore. *J. Phys. Chem. C*, 115:24951–24959, 2011.

[24] Y. He, M. Tsutsui, C. Fan, M. Taniguchi, and T. Kawai. Gate manipulation of DNA capture into nanopores. *ACS Nano*, 5(10):8391–8397, 2011.

[25] J. Newman and W. Tiedemann. Porous-electrode theory with battery applications. *AlChE Journal*, 21:25–41, 1975.

[26] J. R. Melcher and G. I. Taylor. Electrohydrodynamics: A review of the role of interfacial shear stresses. *Annu. Rev. Fluid. Mech.*, 1:111–146, 1969.

[27] D. A. Saville. Electrohydrodynamics: The taylor–melcher leaky dielectric model. *Annu. Rev. Fluid. Mech.*, 29:27–64, 1997.

[28] M. Trau, D. A. Saville, and I. A. Aksay. Assembly of colloidal crystals at electrode interfaces. *Langmuir*, 13:6375–6381, 1997.

[29] W. D. Ristenpart, I. A. Aksay, and D. A. Saville. Assembly of colloidal aggregates by electrohydrodynamic flow: Kinetic experiments and scaling analysis. *Phys. Rev. E*, 69:021405–1–021405–8, 2004.

[30] W. D. Ristenpart, I. A. Aksay, and D. A. Saville. Electrohydrodynamic flow around a colloidal particle near an electrode with an oscillating potential. *J. Fluid. Mech.*, 575:83–109, 2007.

[31] G. Fuhr, T. Schnelle, and B. Wagner. Travelling wave-driven microfabricated electrohydrodynamic pumps for liquids. *J. Micromech. Microeng.*, 4:217–226, 1994.

[32] S. K. Bhaumik, R. Roy, S. Chakraborty, and S. DasGupta. Low-voltage electrohydrodynamic micropumping of emulsions. *Sens. Aactuat. B: Chemical*, 193:288–293, 2014.

[33] B. D. Storey. Direct numerical simulation of electrohydrodynamic flow instabilities in microchannels. *Physica D*, 211:151–167, 2005.

[34] J. C. Ryu, H. J. Park, J. K. Park, and K. H. Kang. New electrohydrodynamic flow caused by the onsager effect. *Phys. Rev. Lett.*, 104:104502–1–104502–4, 2010.

[35] S. Uehara, H. Shintaku, and S. Kawano. Electrokinetic flow dynamics of weakly aggregated λDNA confined in nanochannels. *Trans. ASME: J. Fluid. Eng.*, 133(12):121203–1–121203–8, 2011.

[36] K. Doi, T. Uemura, and S. Kawano. Molecular dynamics study of solvation effect on diffusivity changes of DNA fragments. *J. Mol. Model.*, 17:1457–1465, 2011.

[37] K. Doi, H. Takeuchi, R. Nii, S. Akamatsu, T. Kakizaki, and S. Kawano. Self-assembly of 50 bp poly(da)·poly(dt) DNA on highly oriented pyrolytic graphite via atomic force microscopy observation and molecular dynamics simulation. *J. Chem. Phys.*, 139:085102–1–085102–10, 2013.

[38] R. Mei and R. J. Adrian. Flow past a sphere with an oscillation in the free-stream velocity and unsteady drag at finite reynolds number. *J. Fluid. Mech.*, 237:323–341, 1992.

[39] R. Mei. Flow due to an oscillating sphere and an expression for unsteady drag on the sphere at finite reynolds number. *J. Fluid. Mech.*, 270:133–174, 1994.

[40] R. Mei. Velocity fidelity of flow tracer particles. *Expt. Fluids*, 22:1–13, 1996.

Chapter 3

Observation of Electrohydrodynamic Flow through a Pore in Ion-Exchange Membrane

Abstract

Liquid flows driven by electric force is known as electrohydrodynamics (EHD). EHD flows are expected to be applied to micropumps, microactuators, and mixing devices. However, it is known that conventional EHD flows require at least tens of volts of the applied voltage. In this study, a novel device is developed to generate an EHD flow under a constant current condition with a few voltages. An ion-exchange membrane that has a small pore is set in a reservoir to separate the flow path of anion and cation. The reservoir is filled with NaOH aqueous solution and a constant electric current is applied across the membrane. When the cross sectional area of the ion-exchange membrane is 200 times larger than that of the pore, EHD flows observed in the pore become faster than those in previous studies. The maximum value of the flow velocity reaches 3 mm/s by applying a constant current of 0.8 mA.

Index Terms

Electrohydrodynamics, Ion exchange membrane, Microfluidics, Visualization

3.1 Introduction

Recently nanofabrication techniques have made rapid progresses. In nano-scaled fluidic devices, ion transports strongly affect the liquid flows that often result in complicated flow patterns [1, 25]. Such peculiar flows seem to exceed our understanding by means of conventional ion transport theories [28]. For example, a liquid flow is induced due to high concentrations of electrolyte ions near a charged wall surface when an electric field is externally applied in the solutions as shown in Figure 3-1(a). This kind of flow is known as electroosmotic flow (EOF) [25, 28], as schematically shown Figure 3-1(b). EOFs are one of the hottest topics in micro/nanofluidics and further understanding is required. A charged wall surface in electrolyte solution attracts counter ions and it forms electric double layer (EDL). Particularly, when a distance between two channel wall surfaces becomes closer, EDLs overlap with each other as shown in Figure 3-1(c). In such a narrow channel, electroneutrality is broken and dominant ion transports drive liquid flows. As mentioned above, electrically polarized conditions are inevitable to induce liquid flows by externally applied electric force. In recent, novel technologies to manipulate electrophoretic behavior of single molecules [27, 11, 12], charged particles [7], and allergens [8] by applying EOFs have attracted much attention. Charged molecules, such as deoxyribonucleic acid (DNA) and ribonucleic acid (RNA) in electrolyte solutions are electrically driven by external electric fields. Controlling the transport velocity is crucial to clearly detect a single molecule in extremely narrow spaces, such as nanoslits and nanopores. To do so, a deep understanding of responses of electrolyte ions and liquid flow are inevitable [46]. Electrolyte ions in solutions cause to induce a liquid flow when externally electric force is applied and then, the ions drag surrounding fluids. This flow is called as electrohydrodynamic (EHD) flow [19, 13, 14, 15]. The idea of EHD flows was based on a pioneering work by Melcher and Taylor [19]. Following them, Saville [13] and his coworkers [14, 15] developed the theoretical basis and optically observed the phenomenon. EHD flows are expected to be applied to micropumps and mixing techniques [20]. However, high voltages at least several tens of volts are usually required to make EHD flows. Bhaumik et al. [20] developed a low voltage driving micropump. But, its output flow velocity was lower than the conventional ones, and the flow rate was not enough. For example, they

applied AC fields (15-40 V_{pp}; 5-500 Hz) across the two parallel electrodes. By applying 15 V_{pp}, the velocity of the generated EHD flow resulted in 107 μm/s, in which the distance between the electrodes was set to 600 μm. In this study, we tackle to develop a novel device to investigate EHD flows, which works with moderate currents and voltages. As schematically shown in Figure 3-1(d), an EHD flow passing through a small pore placed in an ion-exchange membrane is optically and electrically measured. Applying an electric current along the channel axis, both the anion and cation are separately attracted to the counter electrodes. In a case using an anion-exchange membrane, anions can pass through all cross-sectional areas including a pore region, but cations are limited to pass through a pore in the membrane. In the experimental system, due to a large difference between a cross-sectional area of anion-exchange membrane and its pore, highly concentrated cations in the pore drive a strong EHD flow. As a result, our device can make a significantly fast EHD flow compared to previous results [20]. Further progresses based on the present results are expected to be developed not only for translocation velocity control of single molecules but also for arbitrary molecular pattern fabrications [15].

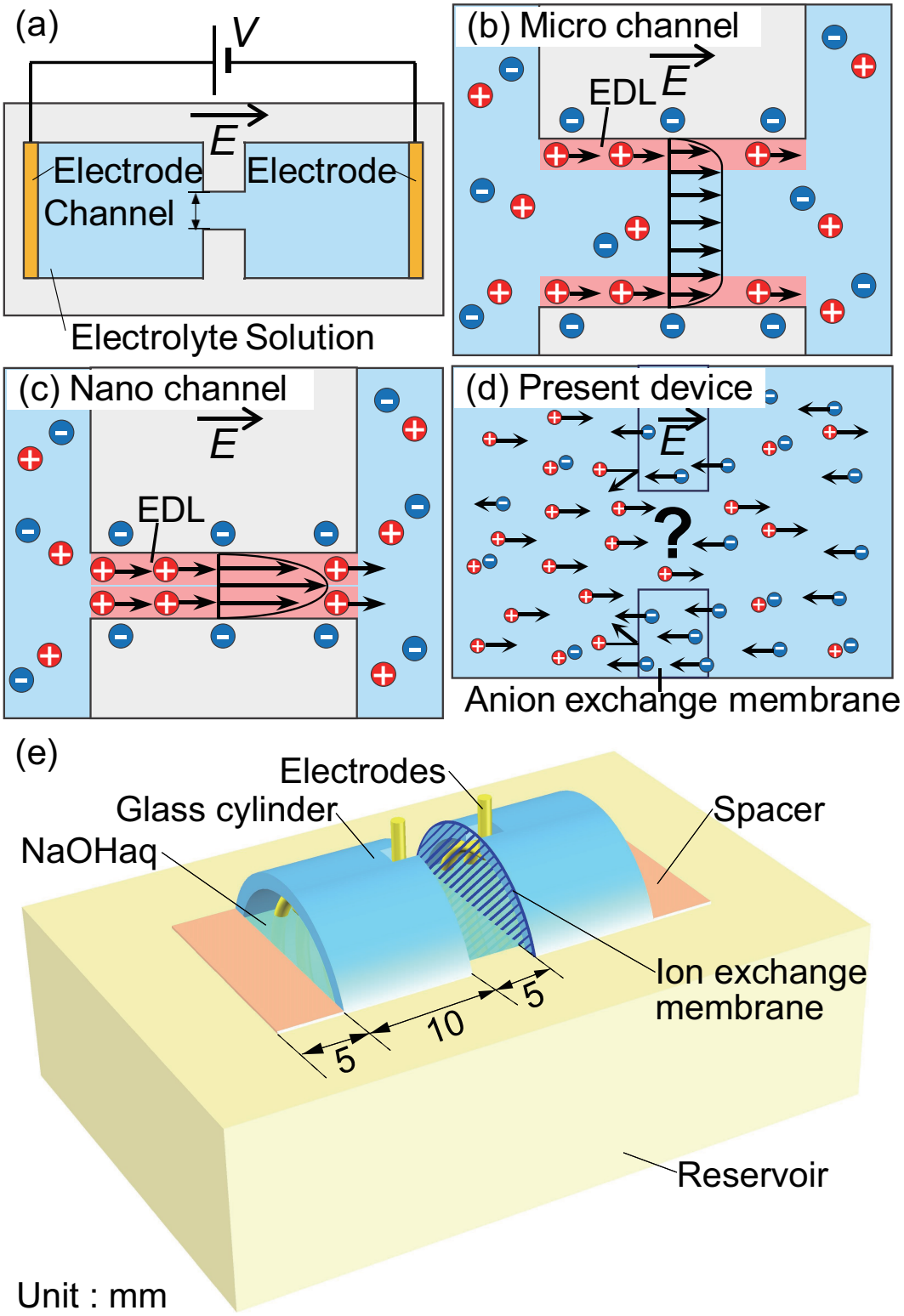

Figure 3-1. Schematic illustrations: (a) whole structure of the experimental system, (b) electroosmotic flow (EOF) in microchannel, (c) EOF in nanochannel, (d) EHD flow in the present system, and (e) design of the present experimental device.

3.2 Experimental Methodology

3.2.1 Design of experimental device

Figure 3-1(e) shows a schematic illustration of the present experimental device. An ion-exchange membrane with a pore and a pair of helical shaped Au electrodes is immersed in a reservoir made of polydimetylsiloxane (PDMS). An anoin-exchange membrane (Neosepta®A-0325, ASTOM Co., Ltd., Tokyo, Japan) was employed in this experiment. The experimental device was designed to set the cross-sectional area of ion-exchange membranes 200 times larger than that of the pore in the membrane, where the ion exchange membranes had a diameter of 18.0 mm. A 1 mm $\times$ 1 mm rectangular cross-section pore was 3 mm in length. This channel was penetrated in the ion-exchange membrane. The system consisted of two different-sized cylindrical chambers: 14.4 and 18.4 mm in diameter. A glass cylindrical chamber (18.0 mm in diameter and 10 mm in length) and a spacer (18.0 mm in diameter and 5mm in length) were placed in both sides of the reservoir to fix an ion-exchange membrane. A 0.83 μm diameter polystyrene particle (Estapor®, MERCK KGaA Co., Ltd., Dermstadt, Germany) was employed as a tracer particle. A 10 volume percent solution of the polystyrene particle was diluted in pure water to 0.1 volume percent, and 200 μL of it was added in 3.6 mL of a 0.1 M NaOH solution for visualization of EHD flows.

3.2.2 Experimental method

Applying a constant current or a constant voltage, electric signals and flow velocities were measured. Behavior of tracer particle in the pore was observed by using a microscope with a high speed camera (VW-9000 Keyence). A constant current of 0.8 mA or a constant voltage of 2.2 V was applied in the solution on the Au electrodes by a potentiostat (VersaSTAT4 AMTEK). Trajectories of the particles were traced at a frame rate of 125 fps and the flow velocity was analyzed. The time response of electric signals was simultaneously measured with a sampling rate of 200 Hz. After the reservoir was filled with the solution, at t = 5, 30, 55, and 80 min, electric force was applied to observe EHD flows. Before the measurements, the electrodes were shorted and the solution was suffi-

ciently stirred to maintain equilibrium.

3.3 Results and Discussion

3.3.1 Confirmation of the experimental condition

Polystyrene particles are usually known to be negatively charged in aqueous solutions and we need to clarify the degree of electric force on polystyrene particles. A 0.1 volume percent solution of the tracer particle was injected near the pore. After the solution was equilibrated, the inside of the pore was observed from the upper side, applying electric potentials up to 5 V for 60 s. As a result, any effective acceleration of the particles by the electric fields could not be found, even though the Brownian motion was clearly observed. Thus, it was concluded that electrophoretic force on the tracer particle was negligibly weak to the applied voltage less than 5 V in this system.

3.3.2 Anion-exchange membrane

Figure 3-2 shows some typical results of the time transition of voltage difference between the electrodes when the constant current of 0.8 mA was applied from $t = 5$ to 35 s. The velocity response of tracer particles was observed in the pore in the anion-exchange membrane. Here, the positive direction of the velocity means a direction along which cations are driven by electrophoresis. As shown in Figure 3-2(a), the flow velocity immediately rose up to 1000 μm/s when the electric current was applied at $t = 5$ s and then, asymptotically approached zero. In Figure 3-2(b), two peaks were observed in the velocity response and there seemed to include different time scales. The velocity reached 1800 μm/s at $t = 6$ s. After that, in the decay process, the second spike was observed at $t = 18$ s. The time constant of the first peak was longer than that of the second one. Figure 3-2(c) shows three peaks over 1000 μm/s. The values were 1000, 1400, and 3000 μm/s at 7.5, 8.5, and 15.5 s, respectively. The velocity of 3000 μm/s was the maximum in this experiment. For the reference, Figure 3-2(d) presents a result in which no effective response was observed, even though the electric current was applied. Weak peaks near 400 μm/s were often observed at $t = 24$ and 27 s. Most of the results indicate that strong liquid flows are

induced when an electric current is applied. Following that, the transient flow velocity is reduced to zero. The reason is that the electric current controls the surface charge of the electrodes; in the same time, almost uniform electric fields expand in the liquid; successively, electrolyte ions respond to the field. Then, surfaces of the electrodes are screened by ions that quickly move very near the electrodes. As shown in Figure 3-2, the voltage response is transient and asymptotically approaches constant values near 2.0-2.5 V. In this period, the behavior of electrolyte ions is drastically modulated to form EDLs and to maintain the constant current condition. That is, ion transports are also excited everywhere in the solution, not only near the electrode surfaces. Gradually forming EDLs, the solution achieves a steady condition. In this process, the current path of cations is limited and highly concentrates in the pore. This is a reason why strong liquid flows are frequently induced along the cation flow direction during the transient response of the voltage difference. In the present system, the constant electric current is maintained by electrolysis of water in the alkaline solution. Then, Na^+ ions, which are finite in the solution, may not be an effective electric carrier to the constant current. Therefore, the velocity response due to the Na^+ transport results in transient. This is the essence of the present EHD flow. In this study, we succeeded to experimentally observe the EHD flow passing through a millimeter-sized pore placed in an anion-exchange membrane. Although nanometer-sized channels are usually required to maintain electrically polarized conditions in liquid phase as shown by the mechanism of EOF (Figures 3-1(a),(b)), our device supposes another method to break the electroneutrality in millimeter-sized spaces.

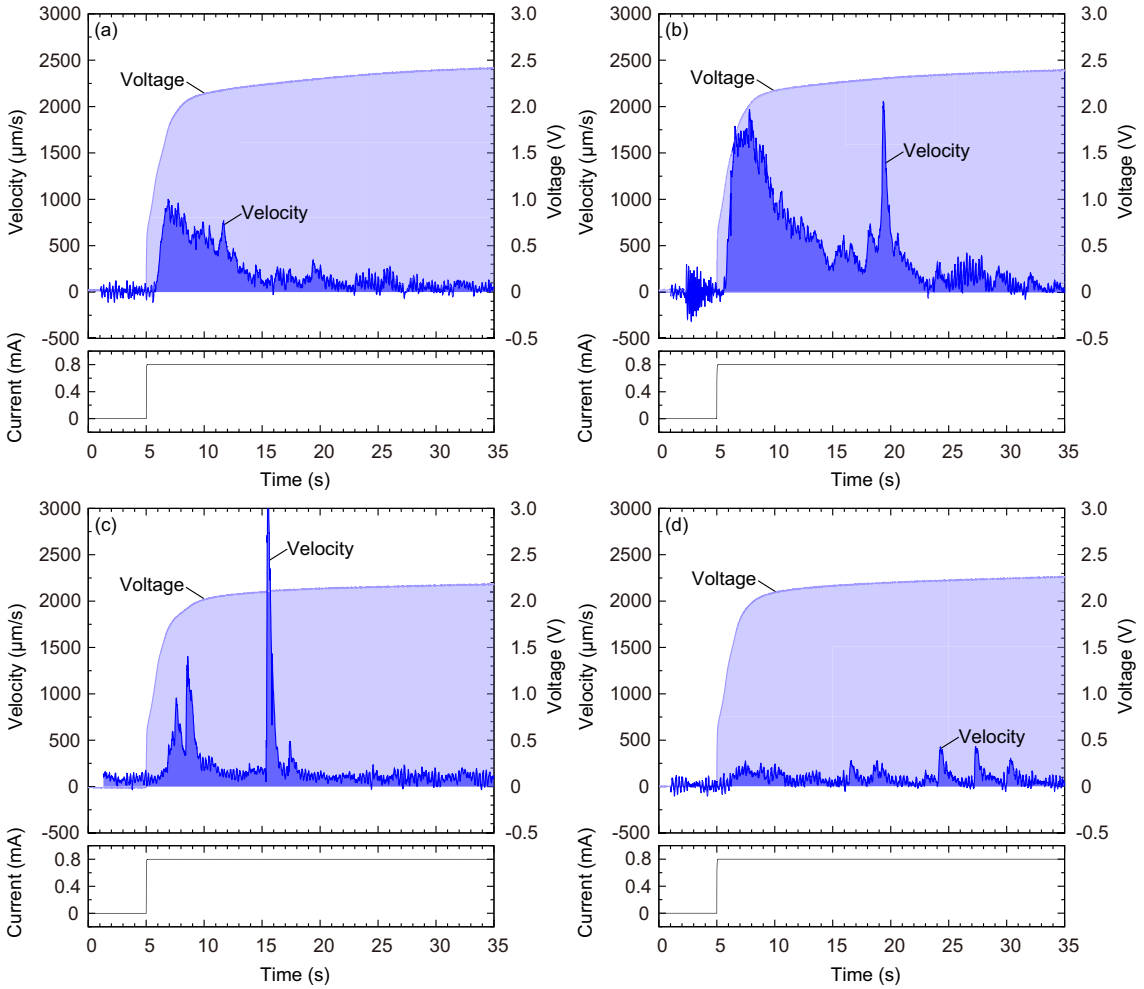

Figure 3-2. Voltage and velocity responses observed in the pore placed in an anion-exchange membrane, where an electric current is applied at t = 5 s. According to transient voltage responses, the velocity presents a variety of responses: (a) a single peak and slow decay to zero, (b) two peaks with different time constants, and (c) two peaks of spike like responses, referring to the case of (d) no prominent responses in the velocity.

3.3.3 EHD generation by applying constant voltages

It was found that EHD flows could be generated by applying a constant electric current and that the direction of observed liquid flows corresponding to that of cation transport. Additionally, we conducted another experiment to clarify that EHD flows could also be induced by applying constant voltages. In Figure 3-2, at the steady states, the voltage response seemed to be settled at 2.0-2.5 V. Referring to this result, a constant voltage difference of 2.2 V was applied on the electrodes. Figure 3-3 shows the response of flow velocity and electric current. The results show a similar velocity response with Figure 3-2. At t = 5 s, the electric potential was externally applied and then, a spike signal of electric current could be observed. Successively, a liquid flow immediately increased and decayed to zero. In the velocity response, many spikes seemed to be included. The mechanism of the EHD flow can be explained in the same manner as the constant current response. To maintain a constant voltage difference between the electrodes, the electric current is controlled against the ionic current in the solution. Thus, the electric current reflects the behavior of ions. According to the ionic response, liquid flow was also induced due to highly concentrated Na+ ions near the pore. Consequently, it was found that both constant current and constant voltage measurements were effective to induce the EHD flows. This result is explained by a theoretical model of liquid flow affected by externally applied electric stresses, which will be reported elsewhere.

3.3.4 Effects of membrane treatments on electric current

To investigate the effects of membrane treatment procedures on the electric current response, we compared three treatment processes. Figure 3-4 shows current response of each membrane with an applied voltage of 2.2 V. In each condition, the electric current response was measured five times for each two membrane and the average values were plotted. The first method is ultrasonic cleaning in pure water. An anion-exchange membrane was immersed in pure water in an ultrasonic cleaner for 10 min twice. In the second method, the membrane was put in NaOH solution for 2 h after the ultrasonic cleaning. In the third method, after the ultrasonic cleaning, the membrane was set in the reservoir and the electric current of 0.8 mA and -0.8 mA were applied to the membrane

for 1 h each direction. In Figure 3-4, peaks, relaxation times, and constant values at the steady current state are compared between the treated membranes mentioned above. The relaxation time τ of electrophoretic mobility μ can be written as $\mu = ze\tau/m$, where z is the valence number, e is the elementary charge, m is the mass. A relationship between the conductance σ and μ is represented by $\sigma = \rho\mu$, where ρ is a charge density. That is, σ is proportional to τ. The longer τ results in the better σ. The anion-exchange membrane was usually kept in 3% NaCl aqueous solution. When the membrane was cleaned in pure water, the conductance tended to decrease because additional ions were removed. Before applying external fields, the long immersion time of the membrane in NaOH solution also improved the σ, because the gradation of electrolytes was equilibrated. As a result, the σ of membranes was improved. Under the applied current condition, ionic current paths actually penetrated the membrane and the σ achieved more preferable conditions. In this case, the τ became the largest among the treatments. This result also indicates that the electric current responses actually reflect the ionic current responses in the solution. This means that the non-equilibrium response of ions in the membrane is actually recognized, even if the membrane is positioned apart from the electrodes. The time transitions of flow velocities, as shown in Figures 3-2 and 3-3, are optically and electrically confirmed to be caused by the ionic motions.

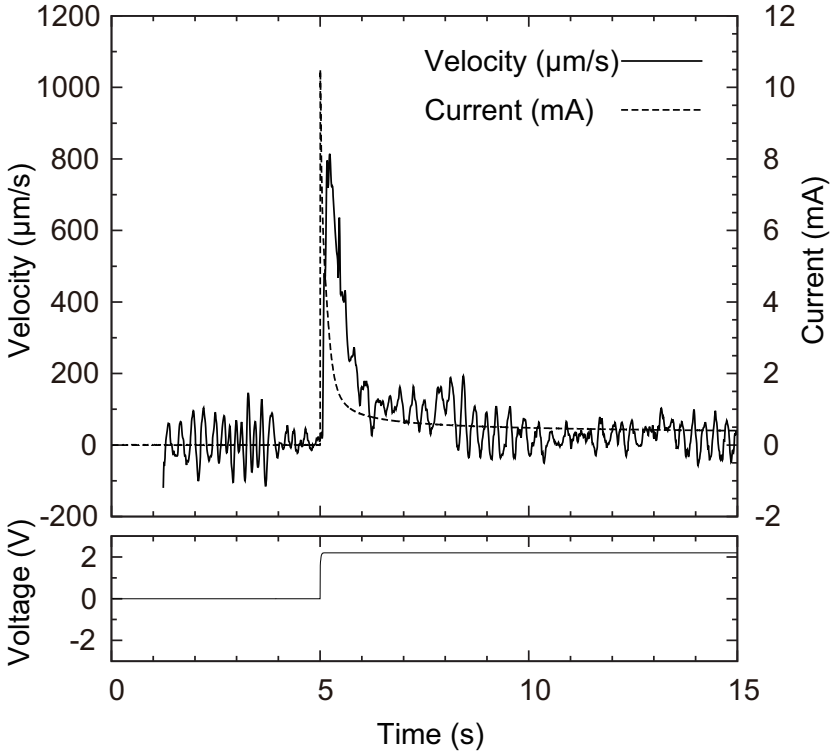

Figure 3-3. Velocity and electric current responses, applying a constant voltage of 2.2 V at t = 5 s. A single sharp peak was found immediately when the voltage was applied.

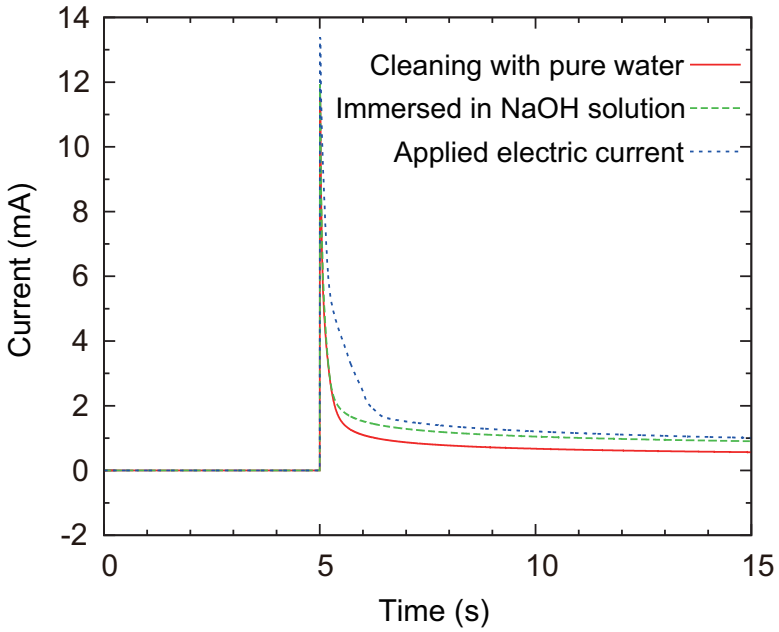

Figure 3-4. Electric current response with respect to different conditions of the membrane.

3.4 Conclusion

In this study, a novel device was developed to observe an EHD flow. Placing a 1-mm scale pore in an anion-exchange membrane, an electrically polarized condition could be generated under a constant current condition. Strong EHD flows were generated in the pore and the maximum flow velocity achieved 3 mm/s. It was confirmed that the EHD flow actually induced along the cation flow direction in a 0.1M NaOH solution. That is, we succeeded to locally visualize the break of electroneutrality in the solution. In the flow velocity responses, the voltage difference asymptotically approached a steady value near 2.0-2.5 V. Furthermore, similar EHD flows could be observed by applying a constant voltage of 2.2 V. In the near future, theoretical results will be reported elsewhere to deeply understand the EHD flow in which a liquid flow is induced by ionic responses according to electric field formations [46].

Bibliography

[1] W. Guan, R. Fan, and M. A. Reed. Field-effect reconfigurable nanofluidic ionic diodes. *Nat. Commun.*, 2:506:1–8, 2011.

[2] H. Daiguji, P. Yang, and A. Majumdar. Ion transport in nanofluidic channels. *Nano Lett.*, 4(1):137–142, 2004.

[3] R. B. Schoch, J. Han, and P. Renaud. Transport phenomena in nanofluidics. *Rev. Mod. Phys.*, 80:839–883, 2008.

[4] S. Uehara, H. Shintaku, and S. Kawano. Electrokinetic flow dynamics of weakly aggregated λDNA confined in nanochannels. *Trans. ASME: J. Fluid. Eng.*, 133(12):121203–1–121203–8, 2011.

[5] T. Yasui, S. Rahong, K. Motoyama, T. Yanagida, Q. Wu, N. Kaji, M. Kanai, K. Doi, K. Nagashima, M. Tokeshi, M. Taniguchi, S. Kawano, T. Kawai, and Y. Baba. Dna manipulation and separation in sublithographic-scale nanowire array. *ACS Nano*, 7(4):3029–3035, 2013.

[6] W. Qian, K. Doi, S. Uehara, K. Morita, and S. Kawano. Theoretical study of the transpore velocity control of single-stranded dna. *Int. J. Mol. Sci.*, 15(8):13817–13832, 2014.

[7] N. Yukimoto, M. Tsutsui, Y. He, H. Shintaku, S. Tanaka, S. Kawano, T. Kawai, and M. Taniguchi. Tracking single-particle dynamics via combined optical and electrical sensing. *Scientific reports*, 3, 2013.

[8] C. Kawaguchi, T. Noda, M. Tsutsui, M. Taniguchi, S. Kawano, and T. Kawai. Electrical detection of single pollen allergen particles using electrode-embedded microchannels. *Journal of Physics: Condensed Matter*, 24(16):164202, 2012.

[9] K. Doi, M. Tsutsui, T. Ohshiro, C.-C. Chien, M. Zwolak, M. Taniguchi, T. Kawai, S. Kawano, and M. Di Ventra. Nonequilibrium ionic response of biased mechanically controllable break junction (MCBJ) electrodes. *J. Phys. Chem. C*, 118:3758–3765, 2014.

[10] J. R. Melcher and G. I. Taylor. Electrohydrodynamics: A review of the role of interfacial shear stresses. *Annu. Rev. Fluid. Mech.*, 1:111–146, 1969.

[11] D. A. Saville. Electrohydrodynamics: The taylor–melcher leaky dielectric model. *Annu. Rev. Fluid. Mech.*, 29:27–64, 1997.

[12] W. D. Ristenpart, I. A. Aksay, and D. A. Saville. Assembly of colloidal aggregates by electrohydrodynamic flow: Kinetic experiments and scaling analysis. *Phys. Rev. E*, 69:021405–1–021405–8, 2004.

[13] W. D. Ristenpart, I. A. Aksay, and D. A. Saville. Electrohydrodynamic flow around a colloidal particle near an electrode with an oscillating potential. *J. Fluid. Mech.*, 575:83–109, 2007.

[14] S. K. Bhaumik, R. Roy, S. Chakraborty, and S. DasGupta. Low-voltage electrohydrodynamic micropumping of emulsions. *Sens. Aactuat. B: Chemical*, 193:288–293, 2014.

[15] K. Doi, H. Takeuchi, R. Nii, S. Akamatsu, T. Kakizaki, and S. Kawano. Self-assembly of 50 bp poly(da)·poly(dt) DNA on highly oriented pyrolytic graphite via atomic force microscopy observation and molecular dynamics simulation. *J. Chem. Phys.*, 139:085102–1–085102–10, 2013.

Chapter 4

Concentration Dependence of Cation-Induced Electrohydrodynamic Flow Passing Through an Anion Exchange Membrane

Abstract

Electrohydrodynamic (EHD) flow is known as a type of liquid flows driven by external electric force. In electrolyte solutions, anions and cations usually interact with each other to maintain electroneutrality. Under such a condition, it is difficult to drive a liquid flow by applying electric potentials on the order of 1 V; at least several tens of volts are required to generate EHD flows, which may not be preferable for aqueous solutions. This study proposes a novel method of inducing a liquid flow passing through a channel with cross-sectional dimensions of 1 mm × 1 mm that is placed in an ion exchange membrane, which performs the function of separating the cation and anion transport pathways. When the optimized design of the experimental apparatus was used, EHD flows were successfully generated in the aqueous solutions by applying a relatively low electric

potential of 2.2 V, and the flow velocity was measured over a wide range of electrolyte concentrations using particle image velocimetry. It was found that high concentration gradients caused the rapid discharge of ions passing through the channel and contributed to achieve a flow speed on the order of 1 mm/s. EHD flows were also theoretically explained using the Navier–Stokes equations to model an ion-drag flow driven by nonequilibrium ion transport in external electric fields. This flow creation method is practical only when ion transport pathways are well controlled and effectively rectified. The present findings will shed light on the development of a promising technology to control liquid flows in multi-scale fluidic channels.

4.1 Introduction

Recently, micro- and nanofluidic devices have attracted significant attention based on expansions in microfabrication technologies, such as micropumps [1, 2, 3, 4, 5, 6], micromixers [7], resistive pulse sensing [8], and single-molecule transport techniques [9, 10, 11, 12]. Particularly, flows driven by external electric forces, which are known as electrohydrodynamic (EHD) flows [13, 14, 15], are a strong candidate for a mass transport method. Stuetzer [16, 17] and Pickard [18] established the principle of ion-drag pumping by injecting electrical charges in liquids to directly drag them using an applied external electric force. Melcher and Taylor [19] also contributed to the development of the EHD theory by realizing a liquid flow created by controlling the concentration gradients of electrical charges in oils. When an electrolyte solution is electrically charged by a difference between the number densities of anions and cations, solvent molecules may be dragged in the direction of dominant ion transport, resulting in a macroscopic liquid flow. However, to induce EHD flows, applied voltages of at least several tens of volts are required to inject electrical charge carriers into liquids using conventional methods [20]. In equilibrated bulk solutions, anions and cations attractively interact with each other to maintain electroneutrality; thus, externally injected energies have to be consumed to ionize solutions. It is difficult to apply such high voltages to aqueous solutions because of the electrolysis of water, which disturbs the precise control of liquid flows.

Channel walls are often electrically charged, particularly in micro- and nanofluidic

channels; this causes counterions to be attracted to the wall surface, where they form an electric double layer (EDL) [21, 22, 23]. When an electric potential is applied, solvents are dragged by highly concentrated counterions. A slip plane is presented at the boundary of the EDL as a result of polarization, meaning plug-like flows can be observed. This type of flow is well known as electroosmotic flow (EOF) [24, 25, 26, 27], which is a liquid flow induced by drag force caused by nonequilibrium ion transport specific in micro- and nanofluidic channels. Such electrokinetic phenomena have also been reviewed in the published literatures [28, 29, 30]. Based on the Helmholtz–Smoluchowski equation [31], a number of numerical studies on EOF in micro- and nano-scale spaces have also been published [32, 33, 34, 35]. EOFs can be driven by low electric potentials and are therefore applicable to flow control in water. Furthermore, electrically charged molecules are also electrophoretically transported in electric fields, and it has been difficult to control molecular transport by EOFs that are limited to low flow rates [36]. In addition to EOFs, EHD flows are expected to contribute to a variety of liquid flow control techniques for practical applications. The reduction of applied electric potentials is inevitable in the employment of EHD flows in aqueous solutions.

To overcome the problems mentioned above, in our previous study, we proposed a novel method of creating EHD flows in a millimeter-scale channel by externally applying a few volts of electric potential, where ion transport pathways were rectified using an ion exchange membrane surrounding the flow channel. In the experiment, to distinguish EHD flows from EOFs, a channel with cross-sectional dimensions of 1 mm × 1 mm was used, because in a channel this large, the apparent EOF caused by ion transport limited in the EDL was negligible. Figure 4-1(a) illustrates the concept of the present system realizing ion flow rectification, in which a flow channel that crosses an anion exchange membrane is immersed in a NaOH solution. When an external electric field is applied across the membrane, the transport of cations is limited through the channel, whereas anions can pass through the entire face of the anion exchange membrane in the reverse direction. Thus, the motion of cations in the narrow channel must be more dominant than that of anions. As a result, a large number of cations that accumulated in the channel actually dragged water molecules and contributed to the induction of a macroscopic liquid flow, which could be optically observed and electrically measured by the experimental

setup used in our previous study [37, 38]. It was figured out that cation transport in alkaline solution preferably induced EHD flows, and the magnitude of the flow velocity reached a value on the order of 1 mm/s [37, 38].

In this study, furthermore, the dependence of EHD flow generation on the concentration of NaOH solution was experimentally and theoretically investigated. By measuring electric potential differences along the flow channel, the transition of the ion concentration was monitored during flow growth. Consequently, it was found that a concentration gradient, which was formed along the channel by applying an electric potential, was immediately relaxed by a generated EHD flow. High-speed flows on the order of 1 mm/s were certainly achieved when the NaOH concentration increased to 0.1 mol/L. Highly concentrated cations were inevitable to drag water molecules in the flow channel because the applied electric energy had to be transferred to a liquid flow effectively via cation transport. The present experimental system used to enhance ion flow rectification enables to create EHD flows in an aqueous solution with an extremely low electrical potential in comparison with that of previous methods [19, 20] and suggests the possibility of novel liquid flow control in micro- and nanofluidics.

4.2 Experimental Methodology

As shown in Figure 4-1(b), the experimental fluid reservoir is filled with a NaOH aqueous solution and is divided into two parts by using an anion exchange membrane (Neosepta® AHA, ASTOM Corp., Tokyo, Japan) [39]. A flow channel with a 1.0 mm × 1.0 mm cross-section and 3.0 mm in length connects the two parts and is acted as the test section in the present experiments. The x axis is defined along the longitudinal direction of the flow channel, and the y and z axes are defined as the horizontal and vertical directions, respectively, as shown in Figure 4-1(b). The origin of the Cartesian coordinate system is set at the center of the channel. The channel walls composed of transparent material are chosen for the clear observation of the tracer particles. This structure allows the observation of liquid flows in the xy plane at $z = 0$ mm by controlling the depth of focus of the microscope used for observation, as shown in Figure 4-1(c). The flow data are independent of x, and the observation point is set to approximately 0.75 mm downstream from the origin, such that $x = 0.75$, $y = 0$, and $z = 0$ mm, as shown in Figure 4-1(b).

Figure 4-1(d) shows photographs of the experimental device and its parts: a membrane, a channel, and Au electrodes. The cross-sectional area of the anion exchange membrane immersed in the solution is set to 10.0 mm × 13.0 mm, and the upper part of the membrane contains a hole with a cross section of 1.0 mm × 1.0 mm, in which the flow channel is set. The surface area of the anion exchange membrane is approximately 130 times larger than that of the channel. The average thickness of the single membrane is 220 μm. The channel walls are made from transparent poly(dimethylsiloxane) (PDMS), and this channel block crosses the membrane. Au-sputtered disk plates are used as the bias electrodes, which are 18.0 mm in diameter and 1.0 mm thick. The fluid reservoir has cross-sectional dimensions of 10.0 mm × 13.0 mm and a length of 30.0 mm. The Au electrodes and anion exchange membrane are fixed to slits at both ends and the center of the reservoir, respectively. For optical observation, polystyrene particles of 2.93 μm in diameter (Estapor®, Merck KGaA, Darmstadt, Germany) are dispersed in the NaOH solution filling the reservoir, where the 1.0 vol% stock solution is diluted to 4.2×10^{-3}

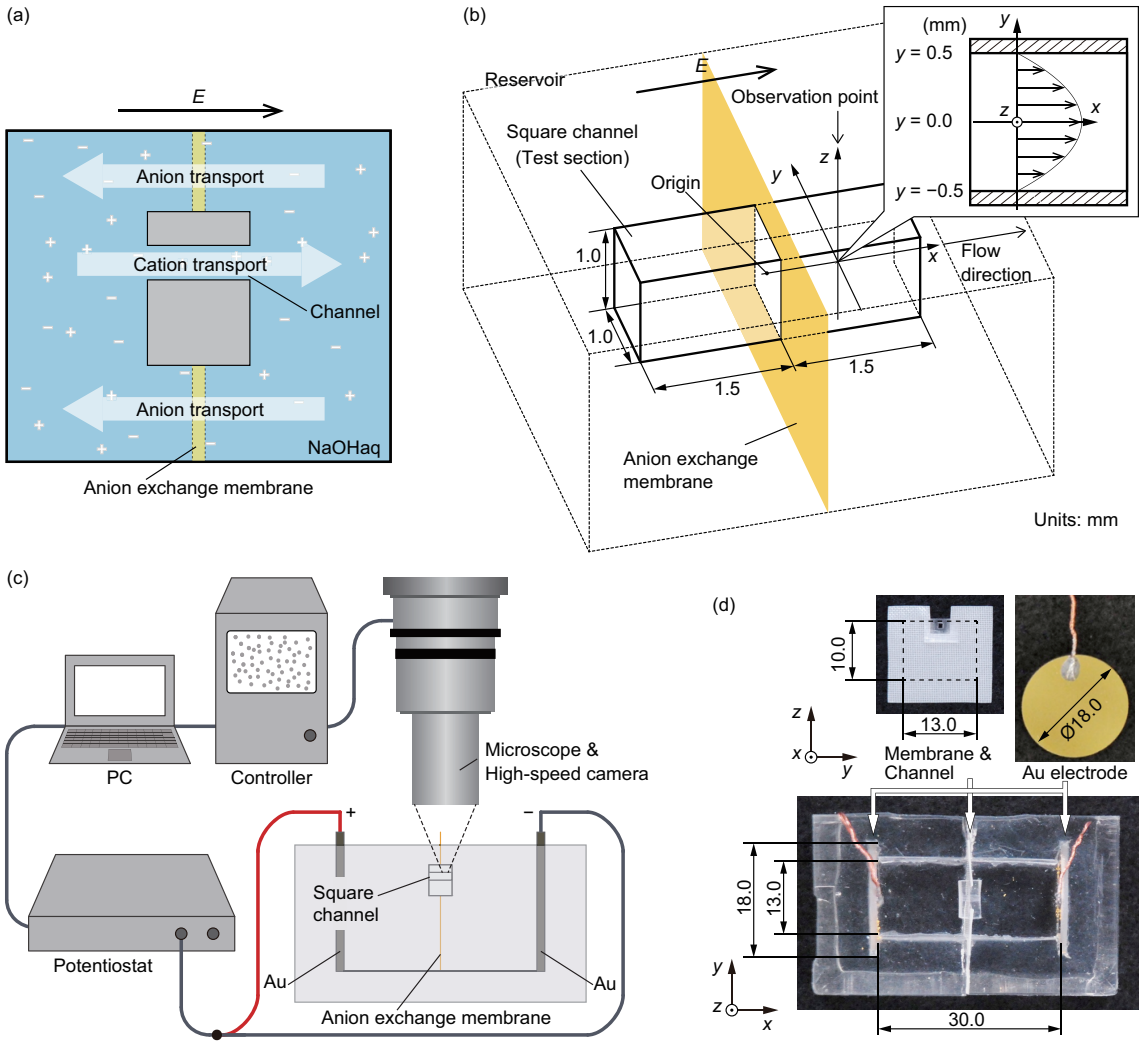

Figure 4-1. (a) Schematic illustration of cation and anion transport, and the pathways of which are separated by an anion exchange membrane. Highly concentrated cations in the channel drag water molecules, generating an EHD flow. (b) Three-dimensional view of a square flow channel with a 1.0 mm × 1.0 mm cross-section and 3.0 mm in length, which crosses the anion exchange membrane and is placed in a reservoir. (c) Schematic illustration of experimental setup. (d) Photographs of the experimental device and its parts: a membrane, a channel, and Au electrodes.

vol%. In this study, the dependence of EHD flow generation on the electrolyte concentration is investigated using NaOH aqueous solutions with concentrations of $C = 1.0 \times 10^{-1}$, 1.0×10^{-2}, and 1.0×10^{-3} mol/L.

The translocation of polystyrene particles is observed and recorded from the upper face of flow channel using a high-speed complementary metal–oxide–semiconductor (CMOS) camera (VW-600M, Keyence Corp., Osaka, Japan) through a microscope (VW-9000, Keyence Corp., Osaka, Japan) with a frame rate of 500 fps and an exposure time of 1.0 ms, as shown in Figure 4-1(c). Assuming that the tracer particles move with the flows without delay because of their small size and negligible surface charge by Debye shielding, the flow field is measured and analyzed using particle image velocimetry (PIV) software (Flownizer 2D, Ditect Co., Ltd., Tokyo, Japan). As a reference for the negative charge of the polystyrene particles in the solution, it was preliminarily confirmed that the electrophoretic motion of the tracer particles, which was two orders of magnitude smaller than that of the observed EHD flows [37], was negligible. Because of the symmetric cross section in the yz plane, velocity profiles are analyzed along the y axis at $z = 0$ mm.

An electric potential of 2.2 V is externally applied to the Au-coated electrodes, and electrical responses are simultaneously monitored using a potentiostat (VersaSTAT4, AMTEK, Inc., Berwyn, PA, USA). This voltage is determined to be the upper limit to avoid generating O_2 and H_2 bubbles by the electrolysis of water, which interrupts accurate observations of EHD flows. Furthermore, voltage differences along the flow channel are measured using Au probes connected to a voltmeter and data logger (NR-500, Keyence Corp., Osaka, Japan) with the distance between the two probes set to 3.0 mm. To confirm that the observed flows are caused by EHD phenomena, an electric potential of 2.2 V is applied for 10 s from $t = 5.00$ to 15.00 s while maintaining a zero potential difference at other times. The electrical measurement is triggered by an electrical signal from the optical observation starting at $t = 0$ s. Before experiments, the anion exchange membrane is ultrasonicated twice in deionized water for 10 min. To maintain the uniformity of the ion distributions, the electrolyte solutions are stirred and the polished electrode surfaces are shorted for over 20 min before each measurement. This preparation process before experimental measurements is based on our past experience; however, it is necessary to realize a stable and reproductive EHD flow and maintain chemical equilibrium at the

beginning of each experiment.

4.3 Results and Discussion

4.3.1 Experimental observations

Using the experimental apparatus described in the previous section, the electrical signals between the two Au electrodes were measured, and the velocity profiles were visualized using the PIV method. Figure 4-2 shows the result obtained using NaOH solutions with concentrations of $C = 1.0 \times 10^{-1}$, 1.0×10^{-2}, and 1.0×10^{-3} mol/L. As shown in Figure 4-2(a), in the case of $C = 1.0 \times 10^{-1}$ mol/L, a liquid flow gradually grew and reached its peak flow velocity at $t = 5.53$ s. After that, the flow decayed until it reached zero velocity at approximately $t = 10.00$ s, although an image of the flow at this time was omitted here. A similar flow pattern was observed for the solution with of $C = 1.0 \times 10^{-2}$ mol/L, as shown in Figure 4-2(b). In this case, however, the peak velocity shown at $t = 6.94$ s was much smaller than that in the former case. In the case of $C = 1.0 \times 10^{-3}$ mol/L, no significant liquid flow was observed, as shown in Figure 4-2(c). Figure 4-2(d) shows the normalized velocity profiles observed at $t = 5.53$ and 6.94 s for the solutions with $C = 1.0 \times 10^{-1}$ and 1.0×10^{-2} mol/L, respectively, where the representative velocity was defined as the velocity at $y = 0$ mm. The results for the two cases with different C show similar flow profiles with no-slip conditions at the wall surfaces, corresponding to a Poiseuille flow in a square duct. The cross-section of the flow channel was square and thus, the flow profile was symmetric along the y and z axes due to the same boundary conditions, because in the present case, the liquid flow was driven by the forces only along the x axis. Consequently, any higher order flow has never been observed, even though we often changed the viewpoints in the z coordinate. This result is later discussed in detail using fluid dynamical analysis. Additionally, the NaOH solutions with higher concentrations show more rapid increases and more significant peaks in their flow velocity responses. The direction of the observed flows corresponds to that of the cation transport, which is a result of the competitive transport of dominant Na^+ and OH^- ions. Here, we do not deny a possibility that the decay of the flow speed beyond the peak shown in Figures 4-2(a) and (b) may be caused by the increase of downstream pressure in the channel as well as de-

pletion of Na^+ ions, if the permeability of the anion exchange membrane is unexpectedly low. In our device, a head difference of about 10 μm is expected when a flow speed of 1 mm/s continues for 1 s. It must prevent the EHD flow, resulting from a rough estimation by Bernoulli's theorem. However, the head variation measured by a laser displacement meter (LK-G5000 and LK-H008W, Keyence Corp., Osaka, Japan) was negligibly small. It might be due to EOF in the reverse direction that was dragged by OH^- ions transported in the membrane [40, 31, 41, 42, 28, 43]. Furthermore, it is possibly within the value estimated by the electrowetting phenomena [44] which is governed by the surface tensions between the gas, solution, and solid wall. In experimental techniques, our own design of the solvent chamber with free surface aims followings. The effects of mass flux and momentum flux owing to the EOF in the membrane are damped at meniscuses and at oscillating surfaces with small amplitudes, respectively. Furthermore, the boundary condition at the free surfaces, which can be set as the zero shear stress, means the surface mobility. In this design, the test section channel set near the free surface should be advantageous to induce the cation-induced EHD flow under the non-equilibrium and non-hydrostatic system between upstream and downstream.

To understand the mechanism of EHD flow generation in detail, we investigated the electric current response I_{Au} at the Au bias electrodes and the voltage difference $\Delta V_{\mathrm{channel}}$ between the probe electrodes at both ends of the test section. The values of I_{Au}, $\Delta V_{\mathrm{channel}}$, and their ratio at their peak point and at $t = 15.00$ s are summarized in Table 4-1. Firstly, we discuss the time evolution of I_{Au} and $\Delta V_{\mathrm{channel}}$ with respect to the flow generation for some typical cases below. After that, the relationship between the ion transport phenomena and EHD flow is discussed later, focusing on the experimental data in Table 4-1.

Figure 4-3 shows the voltage differences V_{Au} between the Au bias electrodes shown in Figure 4-1(d) and the simultaneously measured electric current responses I_{Au} at the same concentrations as in Figure 4-2. The electric current responses were observed to depend on C. In each concentration, spikes were observed immediately after an electric potential was applied. The peak current values were $I_{\mathrm{Au}} = 9.20$, 1.41, and 0.15 mA for $C = 1.0 \times 10^{-1}$, 1.0×10^{-2}, and 1.0×10^{-3} mol/L NaOH, respectively, and were nearly proportional to C. The concentrations of OH^- and Na^+ ions indicate that electrochemical

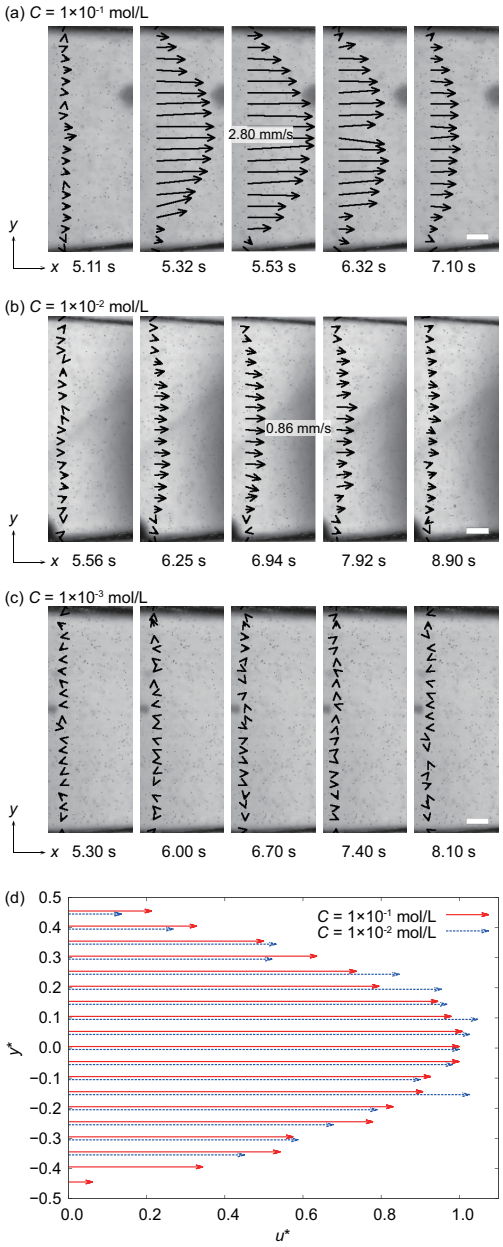

Figure 4-2. Velocity profiles of EHD flows in the xy plane in an electric field along the x axis analyzed using the PIV method for NaOH solutions with C of (a) 1.0×10^{-1} mol/L, (b) 1.0×10^{-2} mol/L, and (c) 1.0×10^{-3} mol/L. The images are composite instantaneous photographs of the particles with the corresponding velocity vectors overlaid on the photographs. An electric potential of 2.2 V was applied at $t = 5.00$ s under each condition. The peak velocity field was observed at $t = 5.53$ and 6.94 s in (a) and (b), respectively. No significant flow was observed in the solution with $C = 1.0 \times 10^{-3}$ mol/L. The arrows in the images show the velocity vectors sampled along the y axis at $x = 0.75$ and $z = 0$ mm. The white scale bars show a length of 100 μm. (d) Normalized velocity profiles at $t = 5.53$ s in (a) (solid vectors in red color) and at $t = 6.94$ s in (b) (dashed vectors in blue color), where y^* and u^* are y normalized by the channel width (1.0 mm) and u normalized by the maximum flow speed at $y = 0$ mm, respectively.

Table 4-1. Experimental data of electric current responses I_{Au} and voltage differences $\Delta V_{\mathrm{channel}}$ between the inlet and outlet of the channel. The maximum, minimum, and average values at the peak and $t = 15$ s were obtained from more than 30 samples at each C. For all data, outlier test with a 5% significance was carried out by applying the modified Thompson-τ method.

		Molarity C of NaOH (mol/L)		
		1.0×10^{-1}	1.0×10^{-2}	1.0×10^{-3}
I_{Au} at peak (mA)	Ave.	8.90 ± 0.74	1.22 ± 0.16	0.151 ± 0.036
	Max.	10.12	1.53	0.184
	Min.	6.99	0.98	0.094
I_{Au} at $t = 15$ s (mA)	Ave.	0.848 ± 0.219	0.277 ± 0.026	0.063 ± 0.010
	Max.	1.22	0.318	0.081
	Min.	0.399	0.204	0.045
$\Delta V_{\mathrm{channel}}$ at peak (mV)	Ave.	565 ± 58	612 ± 34	611 ± 44
	Max.	669	672	682
	Min.	449	544	512
$\Delta V_{\mathrm{channel}}$ at $t = 15$ s (mV)	Ave.	46 ± 12	117 ± 14	253 ± 48
	Max.	68	142	338
	Min.	25	89	142
$I_{\mathrm{Au}}/\Delta V_{\mathrm{channel}}$ at peak (S)		1.5×10^{-2}	2.0×10^{-3}	2.5×10^{-4}
$I_{\mathrm{Au}}/\Delta V_{\mathrm{channel}}$ at $t = 15$ s (S)		1.8×10^{-2}	2.4×10^{-3}	2.5×10^{-4}

reactions at the electrode surfaces and the shielding occur rapidly, and the electric current subsequently converges to a steady state. Because of the electrolysis of water, OH^- and H^+ ions are consumed at the electrodes, resulting in the formation of their concentration gradients. In particular, the transport of OH^- achieves a constant flow because of the electrochemical reaction, which may have triggered an EHD flow through the anion exchange membrane. Anions concentrated in the porous media move dragging solvent molecules and then, an EOF is generated in the membrane [40, 31, 41, 42, 28, 43]. Although this behavior may be a possibility of mass transport in the channel, Na^+ ions also have to dominantly move through the channel toward the cathode to rectify the flow direction. In the present experiment, the flow speed tends to become higher with C. This result cannot be explained by EOF in the membrane alone, because the speed of EOF is known to be proportional to the ζ potential that tends to decrease as C increases due to strong screening of fixed positive charges in the membrane [45, 28]. Figure 4-4 shows

the voltage difference $\Delta V_{\text{channel}}$ between the inlet and outlet of channel measured using probes set at $x = -1.5$ and 1.5 mm on the line $y = z = 0$ mm, corresponding to the velocity profiles in Figure 4-2. In the very early stages after the voltage application, the voltage difference shows a peak value, which may not be strongly dependent on C. As shown in Figure 4-4, peaks of $\Delta V_{\text{channel}}$ = 609, 672, and 642 mV were obtained for $C = 1.0 \times 10^{-1}$, 1.0×10^{-2}, and 1.0×10^{-3} mol/L, respectively. After that, $\Delta V_{\text{channel}}$ decreased rapidly and became almost constant at $t = 15.00$ s depending on C.

According to a previous study [37], the presence of an ionic current in the channel and across the membrane caused the voltage difference to increase. It is supposed that the electric field becomes highly concentrated in the channel as a result of an applied electric potential, which is reduced as the Au electrodes are screened by electrolyte ions. Furthermore, the decay process shows a variety of voltage differences at different C. In each case shown in Figure 4-4, $\Delta V_{\text{channel}}$ approaches to 40, 116, and 245 mV for the solutions with $C = 1.0 \times 10^{-1}$, 1.0×10^{-2}, and 1.0×10^{-3} mol/L, respectively. The experimental data are fit by the superposition of exponential functions with time constants of $\tau_i = 0.01$, 0.02, 0.50, 1, 10, and 100 s in the form of

$$\phi(t) = \sum_i \phi_i e^{-t/\tau_i}, \tag{4-1}$$

where ϕ_i is a coefficient for the time constant τ_i, as listed in Table 4-2. Diffusion coefficients of Na^+ and OH^- are on the order of $D \sim 10^{-9}$ m^2/s and then diffusion in the length of $L \sim 1$ mm takes $\tau = L^2/D \sim 1000$ s at most. In a previous study [46], we found out a power law about the time constant of ionic current affected by electric fields and resulted in $\tau \propto (V/L)^{-2}$. According to this relationship, when $V \sim 100$ mV is applied in the length of $L \sim 1$ mm, we obtain $\tau \sim 0.0001$ s. The sampling rate of electrical measurement, 1000 Hz, limits the minimum value of the time constant at 0.001 s. Based on these rough estimations, the time constants should be in the range from 0.001 s to 1000 s and were further focused to fit the experimental data between 0.01 s and 100 s. As a result, regardless of the molarity of the NaOH solution, the terms with $\tau_i = 0.01$, 0.02, and 0.50 s gave large weights. These fast responses possibly were triggered by electrochemical reactions at the electrode surfaces. Additionally, the behavior governed by the time con-

stants between 1 and 100 s was dependent on C. It was found that the magnitudes of the coefficients tended to shift to larger time constants with decreasing C. In particular, for the solution with $C = 1.0 \times 10^{-3}$ mol/L, much more time passed before the steady state was achieved. Although the transport of Na^+ and OH^- ions was enhanced in the decay process, it was not sufficient to reach the steady state until it took a considerable duration. In contrast, the higher-molarity solutions quickly moderated the ion distributions involving a liquid flow. In other words, the voltage difference across the membrane was relaxed more quickly by flow contributions of many electrolyte ions. $\Delta V_{\mathrm{channel}}$ measured at $t = 15.00$ s increased as C decreased. This means that the resistivity of the solution increases with decreasing C, according to Ohm's law.

Figure 4-5 shows the time evolution of the spatially maximum velocity $u_{\max}$ of the liquid flow observed at approximately $x = 0.75$ and $y = z = 0$ mm, corresponding to the results in Figure 4-2. Each plot point represents the average of successive 25 data points in the time series to smoothen the curves eliminating noise. At $C = 1.0 \times 10^{-1}$ mol/L, as shown in Figure 4-5(a), $u_{\max}$ rapidly increased and reached a peak of 2.80 mm/s at $t = 5.58$ s when an electric potential of 2.2 V was applied. The flow took about 0.58 s after the voltage application to reach its peak in the time evolution. In contrast, for the solution with $C = 1.0 \times 10^{-2}$ mol/L, a peak velocity of $u_{\max} = 0.86$ mm/s was observed at $t = 7.43$ s, as shown in Figure 4-5(b), and a duration of 2.43 s was required for $u_{\max}$ to increase and reach its peak value. This value of $u_{\max}$ in Figure 4-5(b) is three times smaller than that in the former case. This ratio is different from that for maximum I_{Au} that is nearly proportional to C, reflecting the degree of ion flux, as shown in Figures 4-3(a) and (b). $u_{\max}$ is not linearly related to the peak of I_{Au}, although actually the cation transport causes to rectify the EHD flow in the channel. On the other hand, no significant flows were found when using the solution with $C = 1.0 \times 10^{-3}$ mol/L, as shown in Figures 4-2(c) and 4-5(c). In these results, $u_{\max}$ also seems not to depend on the maximum $\Delta V_{\mathrm{channel}}$ shown in Figure 4-4. Therefore, it is suspected that the response of $u_{\max}$ is driven not only by the spike signals of I_{Au} and $\Delta V_{\mathrm{channel}}$ just when an electric potential is applied, but also by the retarded behavior of cations actually enhanced by the applied electric force, involving liquid flows. To compare the response between the liquid and ions to the electric force, their characteristic time can be evaluated as τ_{s} and τ_{e}, respectively,

as follows. In the same length scale L, that of water and electrolyte ions is roughly estimated by the kinematic viscosity $\nu \sim 10^{-6}$ m^2/s and diffusion coefficient $D \sim 10^{-9}$ m^2/s, such that $\tau_e = L^2/D \gg \tau_s = L^2/\nu$, even though ion transport driven by the electrophoretic force shows more rapid responses [46]. Thus, it is suggested that the response of ions is much slower than that of liquid and in other words, an EHD flow that is dragged by ions is seriously affected by the dynamics of ion transport. Table 4-3 presents the average, maximum, and minimum values of u_{max} resulting from the samples in which we could recognize EHD flows in the smoothened experimental data from $t = 5$ to 15 s, such as from the trigger point to the steady state. Here, the cut-off threshold was determined at 0.02 mm/s, because the fluctuations of tracer particles were usually observed within ± 0.02 mm/s regardless of external electric potentials. The probability of significant EHD flows recognized from over 30 samples are also shown. It is confirmed from these results that there is a strong relationship between the flow growth mechanism and C. Thus, this phenomenon is understood as the cation acceleration being translated to an external body force on the liquid from a macroscopic perspective.

Detailed discussions were made about the stability of the EHD phenomena and the measurement uncertainty of the flow velocity in the case of $C = 1 \times 10^{-1}$ mol/L. From the experimental results in 30 runs, EHD flow could be generated stably and the probability of success was about 71% as shown in Table 4-3, however, the variation of the data was relatively large. For example, $u_{max} = 2.80$ mm/s was spatiotemporally in the highest performance and the difference from the mean value was the fraction of 2.68 ($= (2.80 - 0.76)/0.76$). It was the fluctuation of the phenomena, where we could not recognize EHD flows for u_{max} less than 0.02 mm/s from $t = 5$ to 15 s (see Figure 4-5(c)). There is another possibility that the large deviations are mainly caused by the low probability of successfully created EHD flows. Not only u_{max}, but also I_{Au} and $\Delta V_{channel}$ have some deviations and it is suspected that the surfaces of Au electrodes, polished and cleaned before every experiment, were moderately changed with increases in the number of trials. Meanwhile, the present PIV measurements in Figure 4-5(a) were compared with the high-speed observations of the solution dyed by black without polystyrene particles and was in quantitative agreement.

Thus, EHD flow generation driven by applying a low voltage of 2.2 V was success-

fully demonstrated. In particular, the observed Poiseuille flows achieved flow speeds on the order of 1 mm/s in a NaOH solution with a concentration of 1.0×10^{-1} mol/L. As described above, the present experimental device is expected to be applicable to advanced flow control in micro- and nanofluidics, although there remain insufficient conditions to be improved for higher performance, e.g., the dimensions of the flow channel and the precise control of ion concentrations. In our future work, a novel method of measuring the spatiotemporal distributions of the electric potential and current density without disturbing ion and liquid flows will be developed.

4.3.2 Numerical analysis of cation-induced EHD flow

To discuss the transient process in more detail, a mathematical model based on fluid dynamics was developed. This study briefly introduces only the concept of the model; further details of the numerical procedure were already reported by Doi et al. [37]. According to the descriptions above, unsteady, incompressible, and one-directional viscous flows with an applied external body force passing through a square channel with infinite length along the x axis can be described as

$$\rho_m \frac{\partial u}{\partial t} = -\frac{\partial p}{\partial x} + \mu \left(\frac{\partial^2}{\partial y^2} + \frac{\partial^2}{\partial z^2} \right) u + \rho_e E_x, \tag{4-2}$$

where ρ_m is the density of the liquid and ρ_e is the electrical charge density. Taking the divergence of Eq. (4-2), the nonequilibrium electric force and pressure gradient are replaced by

$$-\frac{\partial p}{\partial x} + \rho_e E_x \approx \sum_i f_i e^{-\lambda_i t}, \tag{4-3}$$

where f_i is a constant and the reciprocal of λ_i represents the jth-order time constant. The pressure gradient is caused by the forward and backward flows in the channel and membrane on a continuous surface, respectively, so called internal pressure gradient [47].

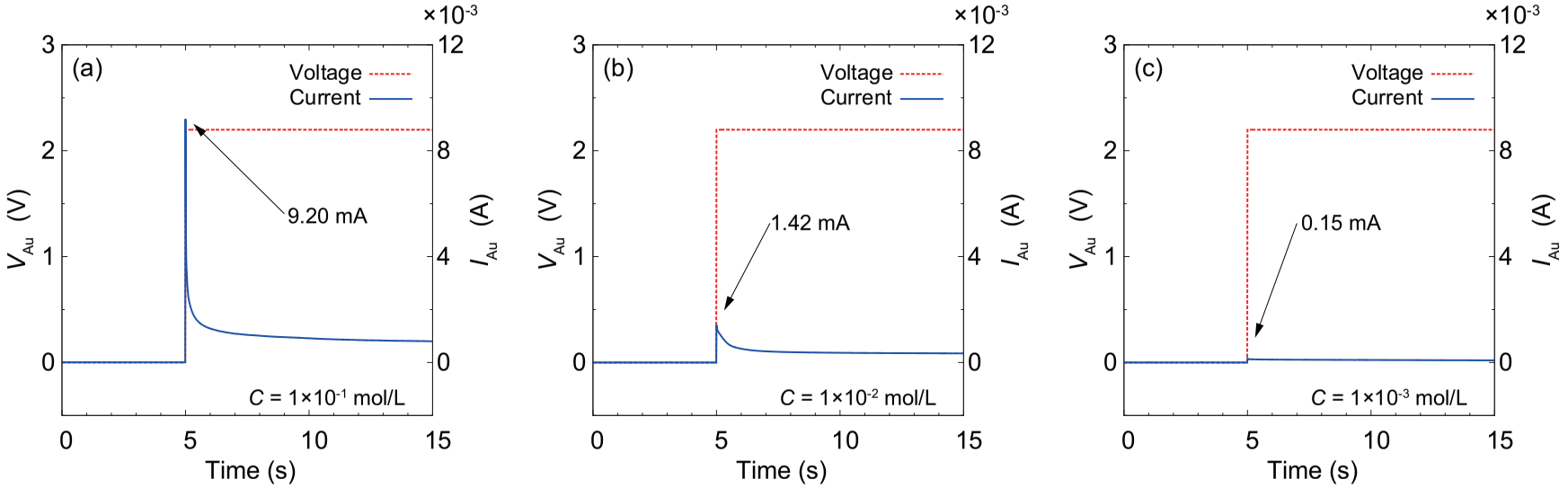

Figure 4-3. Experimental samples of electric current I_{Au} responses (solid lines) to an electric potential V_{Au} (dashed lines) of 2.2 V on Au electrodes applied after $t = 5.00$ s using NaOH solutions with C of (a) 1.0×10^{-1} mol/L, (b) 1.0×10^{-2} mol/L, and (c) 1.0×10^{-3} mol/L. The peaks of I_{Au} were 9.20, 1.42, and 0.15 mA for $C = 1.0 \times 10^{-1}$, 1.0×10^{-2}, and 1.0×10^{-3} mol/L, respectively, and were nearly proportional to C.

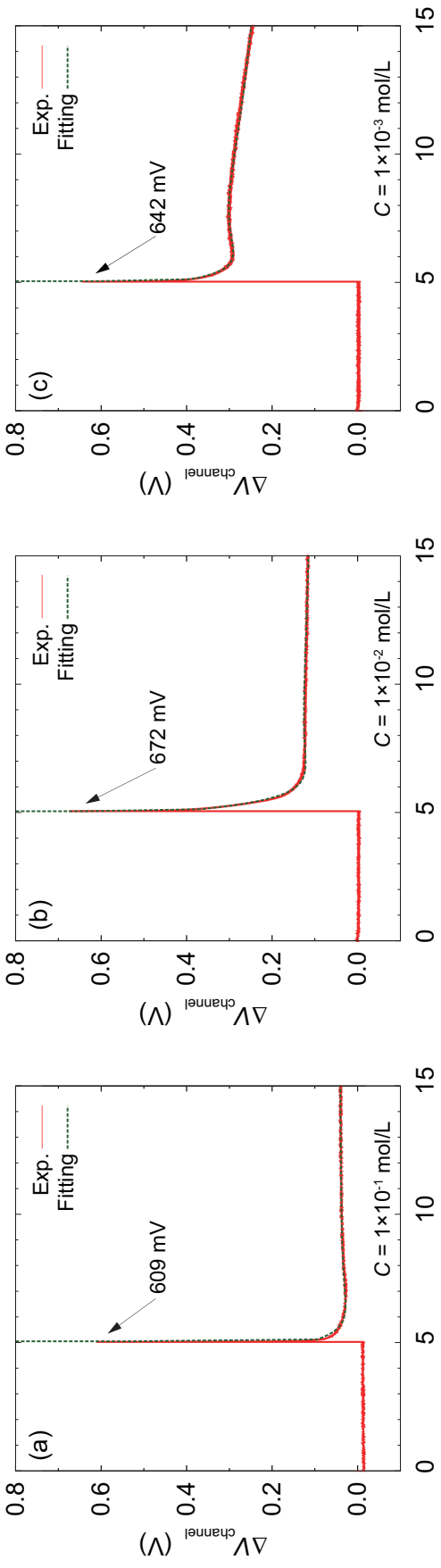

Figure 4-4. Experimental samples of voltage differences $\Delta V_{\text{channel}}$ (solid lines) between the channel inlet and outlet measured using probes with an applied bias voltage of 2.2 V for NaOH samples with C of (a) 1.0×10^{-1} mol/L, (b) 1.0×10^{-2} mol/L, and (c) 1.0×10^{-3} mol/L. Each set of experimental data was fit using Eq. (4-1) (dashed lines), the fitting parameters of which are listed in Table 4-2.

Table 4-2. Coefficient ϕ_i (V) in Eq. (4-1) used to express the response of probe electrodes.

Time constant τ_i (s)	Molarity C of NaOH (mol/L)		
	1.0×10^{-1}	1.0×10^{-2}	1.0×10^{-3}
0.01	0.516	0.238	—
0.02	—	—	0.213
0.50	0.138	0.428	0.303
1	−0.062	−0.152	−0.246
10	−0.011	0.047	0.183
100	0.005	−0.019	−0.070

In the actual system, ρ_e and E_x should be obtained from the ion transport between the electrodes as a numerical solution to both the Poisson equation and the Nernst–Planck equation [46]. However, the present experimental system has a somewhat large length scale to numerically treat the whole system, and thus experimental data are employed to represent the electric force. Here, f_i and λ_i are used as fitting parameters to represent the observed electrical signals. The boundary conditions are

$$u(-l,z,t) = u(l,z,t) = 0, \tag{4-4}$$

$$u(y,-l,t) = u(y,l,t) = 0. \tag{4-5}$$

and the initial velocity is

$$u(y,z,0) = 0, \tag{4-6}$$

Equation (4-2) can be solved to obtain

$$\begin{aligned} u(y,z,t) &= -\frac{16}{\rho_m \pi^2} \sum_{n_y} \sum_{n_z} \sum_{i} \frac{f_i}{(2n_y+1)(2n_z+1)} \\ &\quad \times \frac{e^{-\lambda_i t} - e^{-\lambda_k t}}{\lambda_i - \lambda_k} \sin(k_y y) \sin(k_z z), \end{aligned} \tag{4-7}$$

$$k_y = \frac{(2n_y+1)\pi}{2l}, \quad n_y = 0,1,2,\cdots, \tag{4-8}$$

$$k_z = \frac{(2n_z+1)\pi}{2l}, \quad n_z = 0,1,2,\cdots, \tag{4-9}$$

$$\lambda_k = \frac{(k_y^2 + k_z^2)\mu}{\rho_m}, \tag{4-10}$$

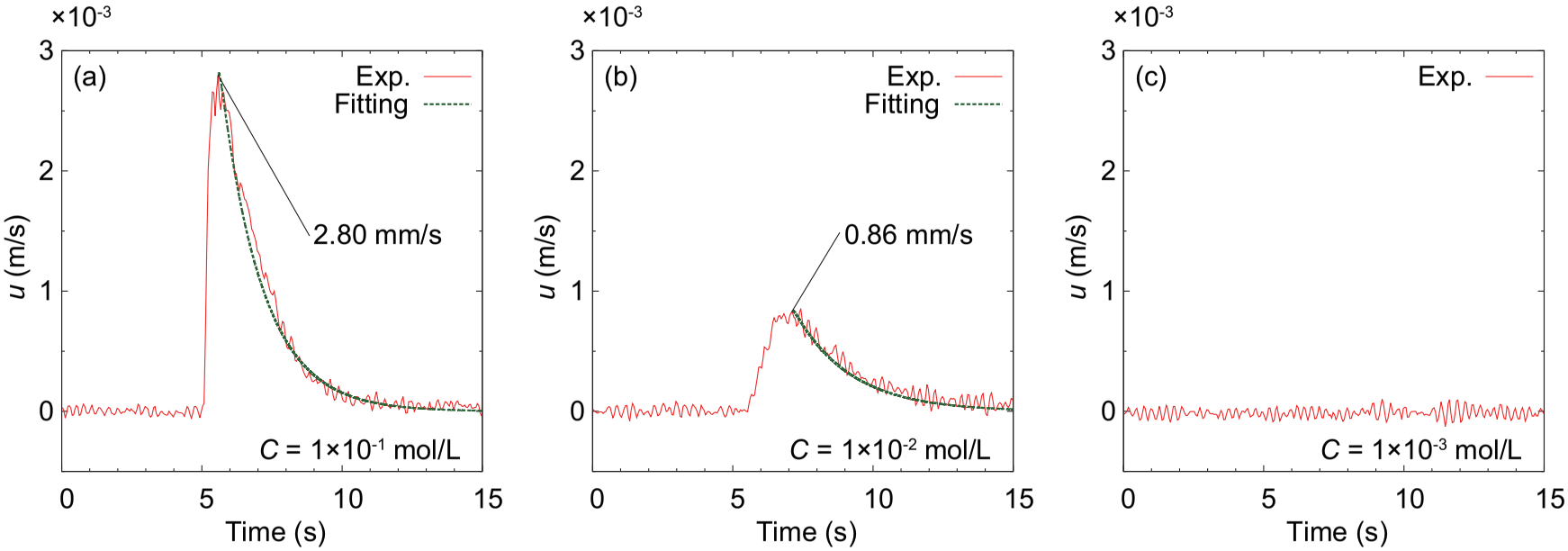

Figure 4-5. Experimental samples of spatially maximum flow velocity $u_{\max}$ responses (solid lines) to an applied potential of 2.2 V at $t = 5.00$ s, using NaOH solutions with C of (a) 1.0×10^{-1} mol/L, (b) 1.0×10^{-2} mol/L, and (c) 1.0×10^{-3} mol/L. The experimental data measured at $x = 0.75$ and $y = z = 0$ mm were fit by Eq. (4-7) (dashed lines), applying Eq. (4-3), and the fitting parameters were determined to reasonably represent the experimental data, particularly behind the peaks, as listed in Table 4-4. No significant flow was observed in the solution with $C = 1.0 \times 10^{-3}$ mol/L.

where the subscript k in Eq. (4-10) is related to n_y and n_z and $2l$ is the length of each side of the square cross-section channel.

The flow structure of an experimentally observed EHD flow was analyzed using Eq. (4-7). Previously, it was confirmed that the duration of the velocity response was on the order of 1 s, resulting from the same dimensions of flow channel as that previously employed immersed in a 1.0×10^{-1} mol/L NaOH solution [37]. According to this knowledge, time constants were defined as $\lambda_i^{-1} = 1.50$ and 2.00 s for $C = 1.0 \times 10^{-1}$ mol/L and $\lambda_i^{-1} = 2.00$ s for $C = 1.0 \times 10^{-2}$ mol/L to fit the decay process of the responses of u, as shown in Figure 4-5(a) and (b), respectively. Here, we focused only on the decay process of u by using the simple model to represent the applied electric force as represented by Eq. (4-3). On the other hand, in the actual process, it is suggested that positive charges diffuse into the channel to reduce the ion concentration difference recognized by $\Delta V_{\text{channel}}$ and consequently, the generated electric body force drives a liquid flow. In comparison between Figures 4-4(a) and 4-5(a), the decay of $\Delta V_{\text{channel}}$ and the rising up of u seem to be synchronized, and also between Figures 4-4(b) and 4-5(b). The acceleration process associated with the diffusion of ions along the x axis is clarified in our future work. As summarized in Table 4-4, for the solution with $C = 1.0 \times 10^{-1}$ mol/L, the calculated coefficients were 38.7 and 4.3 N/m^3 for $\lambda_i^{-1} = 1.50$ and 2.00 s, respectively. For the solution with $C = 1.0 \times 10^{-2}$ mol/L, a coefficient of 12.5 N/m^3 was obtained for $\lambda_i^{-1} = 2.00$ s. These results indicate that the stronger electric force and related internal pressure gradient was quickly applied in the solution of $C = 1.0 \times 10^{-1}$ mol/L NaOH compared with that of $C = 1.0 \times 10^{-2}$ mol/L. However, fitting for the case with $C = 1.0 \times 10^{-3}$ mol/L was omitted because significant flows were hardly observed. The experimental data at various C and their best fit curves are shown in Figure 4-5. A velocity profile along the y axis is also obtained, as shown in Figure 4-6. The numerical results reproduce the velocity decay process observed in the solutions with $C = 1.0 \times 10^{-1}$ and 1.0×10^{-2} mol/L with reasonable accuracy; the case with $C = 1.0 \times 10^{-3}$ mol/L is omitted here. The velocity data show better agreement with the numerical results obtained using the Navier–Stokes equations, strongly suggesting that the trajectories of the tracer particles can be accurately analyzed using the PIV method even near the solid wall and that the Poiseuille flow can be visualized using the tracer particles. It is revealed that the observed liquid flows

are triggered by highly concentrated ion transport exposed to externally applied electric fields and decay as the electric force is reduced.

In Table 4-1, the ratios of $I_{\mathrm{Au}}/\Delta V_{\mathrm{channel}}$ evaluated at the peak point and at t = 15.00 s are also shown, which corresponds to the effective conductivity taking into account the distance between electrodes and the surface area of them. These values must be proportional to C. The ratio linearly increases with C, which is reasonable by means of ionic current conductance, according to Ohm's law. This result suggests that the behavior of ions, which contributes to ionic current passing through the channel, is enhanced behind the peak of I_{Au}. This is a reason why the effective conductance appears to be improved at the steady states especially for the case of $C = 1.0 \times 10^{-1}$ and 1.0×10^{-2} mol/L.

Furthermore, it has been known that ionic current exhibits peculiar current–bias voltage characteristics when ion-selective membranes are used [39, 48, 49]. In particular, ion enrichment and depletion outside the membrane cause ion concentration polarization (ICP) and result in abnormal increases in the current; this is called the "overlimiting" regime [50, 51, 52, 53]. Nonequilibrium processes in ICP may trigger a rectified liquid flow, because ion transport in ion exchange membranes is known to induce EOF to reduce the electric stress, dragging solvent molecules. [39, 28] As shown in Figure 4-7 in a literature [37], the current–voltage characteristics of the anion exchange membrane used in previous experiments actually showed an abnormal trend over a voltage difference of 2 V; additionally, a bias voltage of at least 2.2 V was found to be preferable to induce a liquid flow as examined in this study. The voltage applied across the membrane appears to be in the overlimiting region in comparison with past experimental data [39], which implies a generation of EHD flow in the channel with EOF in the reverse direction through the anion exchange membrane. Although the dynamics of ICP have remained to be considered in the theoretical model in future, the experimental data are accurately fit by the theoretical curve, demonstrating the flow decay process beyond the peaks.

The present results clarify that ion-drag rectification in the channel with cross-sectional dimensions of 1 mm × 1 mm resulted in a Poiseuille flow. The present flow is apparently different from EOF that can be observed in micro- and nanofluidic channels without pressure gradient, resulting from the limitation of the transport of highly concentrated ions near electrically charged channel walls, which usually yields a plug-like

Table 4-3. Average, maximum, and minimum values of $u_{\max}$, resulting from the samples in which EHD flows exceeded the threshold of 0.02 mm/s that could be treated as noise observed regardless of external electric potentials. The probability of significant EHD flow in 30 experimental runs is also presented at the bottom row in percent. In the case of 1.0×10^{-3} mol/L NaOH solution, EHD flow could be recognized once in 30 trials.

		Molarity C of NaOH (mol/L)		
		1.0×10^{-1}	1.0×10^{-2}	1.0×10^{-3}
$u_{\max}$ (mm/s)	Ave.	0.760	0.310	0.383
	Max.	2.80	0.855	—
	Min.	0.190	0.104	—
Ratio of observable flow (%)		71	68	3

Table 4-4. Coefficient f_i (N/m^3) in Eqs. (4-3) and (4-7).

Time constant λ_i^{-1} (s)	Molarity C of NaOH (mol/L)		
	1.0×10^{-1}	1.0×10^{-2}	1.0×10^{-3}
1.50	38.7	—	—
2.00	4.3	12.5	—

flow, as described by the Helmholtz–Smoluchowski equation [31].

Although a complete understanding of the mechanism of EHD flows triggered by the ion transport has not yet been achieved, the rectified ion transport that causes a liquid flow was revealed by the present experimental results. Future work will involve the quantitative clarification of the EHD flow induced by ion transport in nonuniform electric fields and the improvement of the system to achieve a constant flow rate for industrial and/or medical applications.

4.4 Concluding Remarks

In this study, especially focusing on the concentration dependence, ion-drag EHD flow passing through a millimeter-scale flow channel crossing an anion exchange membrane was investigated both experimentally and theoretically. A cation-drag flow was dominantly generated in a channel with cross-sectional dimensions of 1 mm × 1 mm that was placed in an anion exchange membrane to separate cation and anion transport pathways.

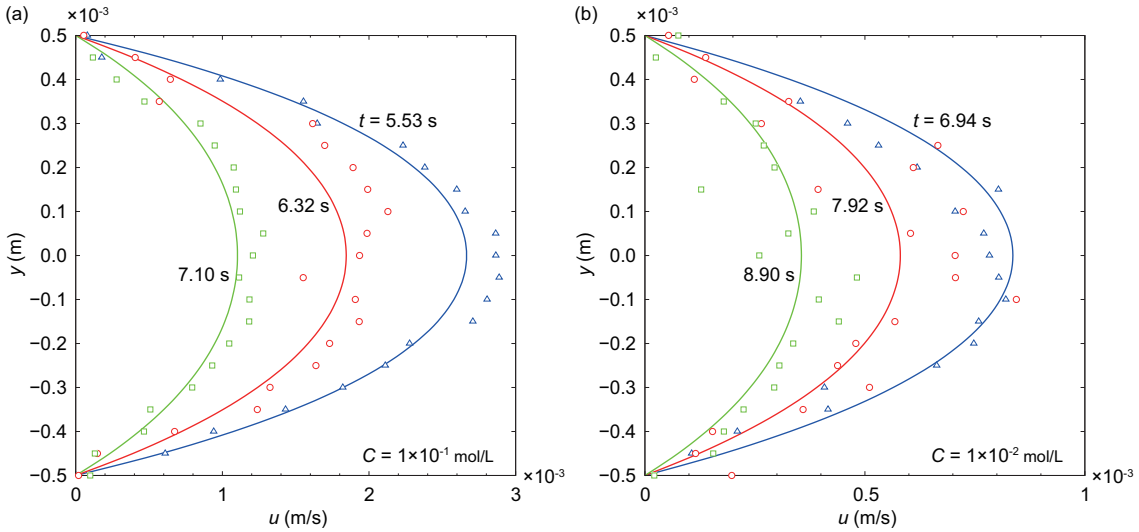

Figure 4-6. Comparison between the velocity fields (symbols) shown in Figure 4-2 and the numerical results (solid lines) from Eq. (4-7) for solutions with C of (a) 1.0×10^{-1} mol/L and (b) 1.0×10^{-2} mol/L. The case of $C = 1.0 \times 10^{-3}$ mol/L was omitted because no significant flow was observed. Experimental data were sampled at $t = 5.53$ (triangle), 6.32 (circle), and 7.10 s (square) in (a) and at $t = 6.94$ (triangle), 7.92 (circle), and 8.90 s (square) in (b).

The velocity field was clearly visualized, and it was confirmed that the direction of the liquid flow actually corresponded to that of cation transport.

The velocity profile closely resembled that of a Poiseuille flow, which is different from the plug-like EOF typically observed in micro- and nanofluidic channels. The flow speed of the EHD flow, which was induced by an applied electric potential of 2.2 V in the NaOH solutions, exceeded 1 mm/s. This technique enabled the induction of electrical charges in aqueous solutions, drastically reducing the magnitude of external electric potentials in comparison with conventional methods.

The concentration dependence of the EHD flow was also investigated using NaOH solutions with concentrations of 1.0×10^{-1}, 1.0×10^{-2}, and 1.0×10^{-3} mol/L. With a 1.0×10^{-1} mol/L NaOH solution, the flow velocity reached the maximum peak speed of 2.80 mm/s with a rapid response to the applied electric potential. However, for the solution with a molarity of 1.0×10^{-2} mol/L, the flow velocity was three times lower than that in the former case, and the flow velocity also increased more slowly. Any significant EHD flow was not observed at a concentration of 1.0×10^{-3} mol/L. It was supposed that ion concentration differences between both ends of the channel, which was detected by the electric potential difference, were reduced and simultaneously a liquid flow appeared to

be developed. The EHD flow was triggered by diffusion and electrophoretic transport of both cations through the channel and anions across the membrane.

The present results demonstrate that EHD flows can be generated in aqueous solutions with relatively low application voltages, and it is expected that such flows will be applied for flow control techniques in multi-scale fluidic channels.

Bibliography

[1] S. Zeng, C.-H. Chen, J. C. Mikkelsen, and J. G. Santiago. Fabrication and characterization of electroosmotic micropumps. *Sens. Actuat. B*, 79(2):107–114, 2001.

[2] A. Brask, G. Goranović, M. J. Jensen, and H. Bruus. A novel electro-osmotic pump design for nonconducting liquids: theoretical analysis of flow rate–pressure characteristics and stability. *J. Micromech. Microeng.*, 15(4):883, 2005.

[3] Y. S. Kim, J. H. Kim, K. H. Na, and K. Rhee. Experimental and numerical studies on the performance of a polydimethylsiloxane valveless micropump. *Proc. Inst. Mech. Eng. C: J. Mech. Eng. Sci.*, 219(10):1139–1145, 2005.

[4] K.-S. Yun, I.-J. Cho, J.-U. Bu, C.-J. Kim, and E. Yoon. A surface-tension driven micropump for low-voltage and low-power operations. *J. Microelectromech. Sys.*, 11(5):454–461, 2002.

[5] O. O. Osman, H. Shintaku, and S. Kawano. Development of micro-vibrating flow pumps using MEMS technologies. *Microfluid. Nanofluid.*, 13(5):703–713, 2012.

[6] O. O. Osman, A. Shirai, and S. Kawano. A numerical study on the performance of micro-vibrating flow pumps using the immersed boundary method. *Microfluid. Nanofluid.*, 19(3):595–608, 2015.

[7] A. O. El Moctar, N. Aubry, and J. Batton. Electro-hydrodynamic micro-fluidic mixer. *Lab Chip*, 3(4):273–280, 2003.

[8] J. Menestrina, C. Yang, M. Schiel, I. Vlassiouk, and Z. S. Siwy. Charged particles modulate local ionic concentrations and cause formation of positive peaks in resistive-pulse-based detection. *J. Phys. Chem. C*, 118:2391–2398, 2014.

[9] C. Dekker. Solid-state nanopores. *Nat. Nanotechnol.*, 2:209–215, 2007.

[10] B. M. Venkatesan and R. Bashir. Nanopore sensors for nucleic acid analysis. *Nat. Nanotechnol.*, 6:615–624, 2011.

[11] T. Yasui, S. Rahong, K. Motoyama, T. Yanagida, Q. Wu, N. Kaji, M. Kanai, K. Doi, K. Nagashima, M. Tokeshi, M. Taniguchi, S. Kawano, T. Kawai, and Y. Baba. Dna manipulation and separation in sublithographic-scale nanowire array. *ACS Nano*, 7(4):3029–3035, 2013.

[12] W. Qian, K. Doi, S. Uehara, K. Morita, and S. Kawano. Theoretical study of the transpore velocity control of single-stranded dna. *Int. J. Mol. Sci.*, 15(8):13817–13832, 2014.

[13] D. A. Saville. Electrohydrodynamics: The taylor–melcher leaky dielectric model. *Annu. Rev. Fluid. Mech.*, 29:27–64, 1997.

[14] W. D. Ristenpart, I. A. Aksay, and D. A. Saville. Assembly of colloidal aggregates by electrohydrodynamic flow: Kinetic experiments and scaling analysis. *Phys. Rev. E*, 69:021405–1–021405–8, 2004.

[15] W. D. Ristenpart, I. A. Aksay, and D. A. Saville. Electrohydrodynamic flow around a colloidal particle near an electrode with an oscillating potential. *J. Fluid. Mech.*, 575:83–109, 2007.

[16] O. M. Stuetzer. Ion drag pressure generation. *J. Appl. Phys.*, 30:984–994, 1959.

[17] O. M. Stuetzer. Ion drag pumps. *J. Appl. Phys.*, 31:136–146, 1960.

[18] W. F. Pickard. Ion drag pumping. i. theory. *J. Appl. Phys.*, 32:246–250, 1963.

[19] J. R. Melcher and G. I. Taylor. Electrohydrodynamics: A review of the role of interfacial shear stresses. *Annu. Rev. Fluid. Mech.*, 1:111–146, 1969.

[20] S. K. Bhaumik, R. Roy, S. Chakraborty, and S. DasGupta. Low-voltage electrohydrodynamic micropumping of emulsions. *Sens. Aactuat. B: Chemical*, 193:288–293, 2014.

[21] D. Stein, M. Kruithof, and C. Dekker. Surface-charge-governed ion transport in nanofluidic channels. *Phys. Rev, Lett.*, 93(3):035901, 2004.

[22] R. B. Schoch, J. Hann, and P. Renaud. Effect of the surface charge on ion transport through nanoslits. *Phys. Fluids*, 17:100604–1–100604–5, 2005.

[23] W. Guan and M. A. Reed. Electric field modulation of the membrane potential in solid-state ion channels. *Nano Lett.*, 12:6441–6447, 2012.

[24] D. Ross, T. J. Johnson, and L. E. Locascio. Imaging of electroosmotic flow in plastic microchannels. *Anal. Chem.*, 73(11):2509–2515, 2001.

[25] H. Daiguji, P. Yang, and A. Majumdar. Ion transport in nanofluidic channels. *Nano Lett.*, 4(1):137–142, 2004.

[26] S.-S. Hsieh, H.-C. Lin, and C.-Y. Lin. Electroosmotic flow velocity measurements in a square microchannel. *Colloid Polym. Sci.*, 284(11):1275–1286, 2006.

[27] S. Uehara, H. Shintaku, and S. Kawano. Electrokinetic flow dynamics of weakly aggregated λDNA confined in nanochannels. *Trans. ASME: J. Fluid. Eng.*, 133(12):121203–1–121203–8, 2011.

[28] R. B. Schoch, J. Han, and P. Renaud. Transport phenomena in nanofluidics. *Rev. Mod. Phys.*, 80:839–883, 2008.

[29] W. Sparreboom, A. van den Berg, and J. C. T. Eijkel. Principles and applications of nanofluidic transport. *Nat. Nanotechnol.*, 4:713–720, 2009.

[30] H. Daiguji. Ion transport in nanofluidic channels. *Chem. Soc. Rev.*, 39:901–911, 2010.

[31] A. J. Bard and L. R. Faulkner. *Electrochemical methods, 2nd Ed.*, pages 362–363. John Wiley & Sons, Danvers, MA, USA, 2001.

[32] B. Zhang, Y. Ai, J. Liu, S. W. Joo, and S. Qian. Polarization effect of a dielectric membrane on the ionic current rectification in a conical nanopore. *J. Phys. Chem. C*, 115:24951–24959, 2011.

[33] M. Zhang, L.-H. Yeh, S. Qian, J.-P. Hsu, and S. W. Joo. DNA electrokinetic translocation through a nanopore: Local permittivity environment effect. *J. Phys. Chem. C*, 116:4793–4801, 2012.

[34] Y. He, M. Tsutsui, C. Fan, M. Taniguchi, and T. Kawai. Controlling DNA translocation through gate modulation of nanopore wall surface charges. *ACS Nano*, 5:5509–5518, 2011.

[35] Y. He, M. Tsutsui, C. Fan, M. Taniguchi, and T. Kawai. Gate manipulation of DNA capture into nanopores. *ACS Nano*, 5:8391–8397, 2011.

[36] Y. Takamura, H. Onoda, H. Inokuchi, S. Adachi, A. Oki, and Y. Horiike. Low-voltage electroosmosis pump for stand-alone microfluidics devices. *Electrophoresis*, 24(1-2):185–192, 2003.

[37] K. Doi, A. Yano, and S. Kawano. Electrohydrodynamic flow through a 1 mm^2 cross-section pore placed in an ion-exchange membrane. *J. Phys. Chem. B*, 119(1):228–237, 2015.

[38] A. Yano, K. Doi, and S. Kawano. Observation of electrohydrodynamic flow through a pore in ion-exchange membrane. *Int. J. Chem. Eng. Appl.*, 6(4):254, 2015.

[39] J. J. Krol, M. Wessling, and H. Strathmann. Concentration polarization with monopolar ion exchange membranes: current-voltage curves and water dissociation. *J. Mem. Sci.*, 162:145–154, 1999.

[40] M. W. Verbugge and R. F. Hill. Ion and solvent transport in ion-exchange membranes. i. a macrohomogeneous mathematical model. *J. Electrochem. Soc.*, 137(3):886–893, 1990.

[41] K. Kopecka, G. Drouin, and G. W. Slater. Capillary electrophoresis sequencing of small ssdna molecules versus the ogston regime: Fitting data and interpreting parameters. *Electrophoresis*, 25:2177–2185, 2004.

[42] C.-Y. Wang. Fundamental models for fuel cell engineering. *Chem. Rev.*, 104:4727–4766, 2004.

[43] K. D. Dorfman. Dna electrophoresis in microfabricated devices. *Rev. Mod. Phys.*, 82(4):2903–2947, 2010.

[44] H. Shintaku, Y. Tatara, and S. Kawano. Droplet transportation on vertical parallel electrodes using electrowetting and interfacial oscillation. *J. Fluid Sci. Technol.*, 4(3):636–647, 2009.

[45] J. Lyklema and J. Th. G. Overbeek. On the interpretation of electrokinetic potentials. *J. Colloid Sci.*, 16:501–512, 1961.

[46] K. Doi, M. Tsutsui, T. Ohshiro, C.-C. Chien, M. Zwolak, M. Taniguchi, T. Kawai, S. Kawano, and M. Di Ventra. Nonequilibrium ionic response of biased mechanically controllable break junction (MCBJ) electrodes. *J. Phys. Chem. C*, 118:3758–3765, 2014.

[47] S. Devasenathipathy, R. Bharadwaj, and J. G. Santiago. Investigation of internal pressure gradients generated in electrokinetic flows with axial conductivity gradients. *Exp. Fluids*, 43:959–967, 2007.

[48] I. Rubinstein and B. Zaltzman. Electro-osmotically induced convection at a permselective membrane. *Phys. Rev. E*, 62(2):2238–2251, 2000.

[49] M. B. Andersen, D. M. Rogers, J. Mai, B. Schudel, A. V. Hatch, S. B. Rempe, and A. Mani. Spatiotemporal ph dynamics in concentration polarization near ion-selective membranes. *Langmuir*, 30:7902–7912, 2014.

[50] T. A. Zangle, A. Mani, and J. G. Santiago. Theory and experiments of concentration polarization and ion focusing at microchannel and nanochannel interfaces. *Chem. Soc. Rev.*, 39:1014–1035, 2010.

[51] Y.-A. Song S. J. Kim and J. Han. Nanofluidic concentration devices for biomolecules utilizing ion concentration polarization: theory, fabrication, and applications. *Chem. Soc. Rev.*, 39:912–922, 2010.

[52] R. K. Anand, E. Sheridan, K. N. Knust, and R. M. Crooks. Bipolar electrode focusing: Faradaic ion concentration polarization. *Anal. Chem.*, 83:2351–2358, 2011.

[53] L.-H. Yeh, M. Zhang, S. Qian, J.-P. Hsu, and S. Tseng. Ion concentration polarization in polyelectrolyte-modified nanopores. *J. Phys. Chem. C*, 116:8672–8677, 2012.

Chapter 5

General Conclusion

In this thesis, it was suggested that the rectification of ion transport pathways was an effective way to generate a locally polarized condition in liquid. Using a NaOH aqueous solution that was separated by an anion exchange membrane, a liquid flow was driven by the rectified ionic currents, which was visualized focusing on the flow channel placed in the membrane. In Chapter 2, a basic principle of EHD flow was examined in rectified ionic current conditions, where the rectification of liquid flows induced by both a cation current in the flow channel and an anion current in an anion exchange membrane were theoretically modeled and experimentally observed. In the theoretical model, a liquid driven by electrical forces was expressed by Navier-Stokes equations in which ionic responses in non-uniform electric fields were taken into account. It was elucidated that the rectification of ionic currents using an ion exchange membrane resulted in the drastic reduction of electric potentials that was externally applied to drive the EHD flow. The flow velocity on the order of 1 mm/s was achieved by applying an electric potential of 2.2 V. To the constant applied voltage, the electric current transiently decayed and converged to a steady current. It was also clarified that the EHD flow quickly responded to the electric body force by changing the direction. The experimental results qualitatively agreed with the numerical analysis and on the other hand, the delay in the EHD flow response to the electrical signals was not clarified quantitatively. It was suggested that long time responses of actual EHD flows were caused by non-equilibrium ion distributions that were gradually modified after applying electric potentials. In Chapter 3, a constant current condition was examined to generate EHD flows. The constant current of 0.8 mA resulted

in the similar trends with a constant voltage condition. In the present system, a steady current seemed to be mainly maintained by the water electrolysis and OH^- current. The electric current and ionic current were exchanged via the electrochemical reactions on the electrode surfaces. It was found that a constant current was also maintained in the flow channel and that rectified cation transport caused to induce the electric force in the liquid. In Chapter 4, a relationship between the ion concentration and flow velocity was investigated. Using a variety of 1.0×10^{-1}, 1.0×10^{-2}, and 1.0×10^{-3} mol/L NaOH solutions, velocity profiles were visualized and analyzed. It was found that the flow velocity increased with increasing the concentrations. When applying an electric potential, rapid increase in the electric potential difference was found between both ends of the channel, where the potential difference was successively decayed. The magnitude of changes in the potential difference became higher with increasing the concentrations. According to this trend, the peak of EHD flow also became higher with the concentrations. Furthermore, the decay time tended to be longer in the lower concentrations. It was concluded that the response of the electric potential difference reflected the ion transport process near and in the channel. After applying an electric potential, Na^+ ions transported and formed the difference in the concentration between both ends of the channel, which was resulted from the electric potential difference. Next, the concentration gradient was relaxed and an EHD flow was induced as Na^+ ions passed through the channel, where the number of cations in the channel depended on the concentrations. Observed velocity profile showed similar shape to Poiseuille flow, which was different from plug-like flow induced by EOF in micro- and nanochannels. The present results indicate that this kind of flow may be preferable to control liquid flows in multi-scale fluidic channels because such a Poiseuille flow field possibly generates a pressure gradient that effectively transport liquids in narrower spaces.

In the next stage, pressure gradients induced by the ion-drag EHD flow have to be measured. Although we did not succeed to clarify the presence of pressure gradients in this thesis, to make it apparent some additional improvements are inevitable. For instance, fine tuning of the liquid quantity is required; charge carrier ions have to be constantly introduced into the test section in a narrow channel; optimal ion concentrations have to be prepared carefully. Solving these problems, electrical body forces applied in

liquid are efficiently transfer to pressure gradients that can be measured quantitatively. These important topics have remained to be solved in the near future.

EHD flows have been applied in various technologies, since an ion-drag EHD pump was invented by Stuetzer in 1959. Although there was a demerit that the conventional EHD pumps required excessively high electric potentials to inject electrical charges into the solvents, the present results enable us to use the EHD flows in aqueous solutions by reducing the bias voltages. The present results will open the door of technological frontiers using EHD flows in aqueous solutions, such as transport techniques of biomacromolecules and biological batteries mimicking the mechanism of biological cell membranes.

List of Publication

Journal Articles

[1] Kentaro DOI, Ayako YANO, and Satoyuki KAWANO,“Electrohydrodynamic Flow through a 1 mm^2 Cross-Section Pore Placed in an Ion-Exchange Membrane”, The Journal of Physical Chemistry B, Vol. 119, pp. 228-237, (2014).

[2] Ayako YANO, Kentaro DOI, and Satoyuki KAWANO,“Observation of Electrohydrodynamic Flow through a Pore in Ion-Exchange Membrane”, International Journal of Chemical Engineering and Applications, Vol. 6, pp. 254-257, (2015).

[3] Ayako Yano, Hiroki Shirai, Moino Imoto, Kentaro Doi and Satoyuki Kawano, "Concentration Dependence of Cation-Induced Electrohydrodynamic Flow Passing Through an Anion Exchange Membrane," Japanese Journal of Applied Physics, in press.

International Conference Proceedings

[1] Ayako YANO, Kentaro DOI, and Satoyuki KAWANO,“Response of ion-induced EHD flow to ac electric fields”, 13th International Conference on Flow Dynamics, OS6-15, pp. 338-339, Miyagi, Japan, October (2016).

[2] Ayako YANO, Kentaro DOI, and Satoyuki KAWANO,“Measurement of pulsating EHD flow driven by AC electric fields”, International Symposium on Micro-Nano Science and Technology 2016, pp. 36, Tokyo, Japan, December (2016).

Domestic Conference Proceedings

[1] 矢野絢子，土井謙太郎，川野聡恭，電解質溶液における非定常イオン流の可視化，日本機械学会 2014 年度年次大会講演論文集 DVD － ROM，p.J0550302，東京，2014 年 9 月.

[2] 矢野絢子，土井謙太郎，川野聡恭，電解質溶液におけるイオン流動現象の可視化観察，日本機械学会 第 92 期 流体工学部門講演会，USB，1310，富山，2014 年 10 月．

[3] 矢野絢子，土井謙太郎，川野聡恭，イオン交換膜を介した EHD 流れの可視化および電気計測，日本機械学会 関西支部 第 90 期定時総会講演会 講演論文集，p. 395，京都，2015 年 3 月．

[4] 矢野絢子，土井謙太郎，川野聡恭，細孔に誘起される EHD 流の定量的評価，日本機械学会 2015 年度年次大会講演論文集 DVD － ROM，p.J0540201，北海道，2015 年 9 月．

[5] 矢野絢子，土井謙太郎，川野聡恭，交流電場に誘起されるアルカリ溶液の ion-induced EHD 流れ，日本機械学会 2016 年度年次大会講演論文集 DVD － ROM，p.J0540106，福岡，2016 年 9 月．

[6] 矢野絢子，名倉諒，二戸郁賀，土井謙太郎，辻徹郎，川野聡恭，電気流体力学流れによる粒子運動の制御,「光圧によるナノ物質操作と秩序の創生」第一回公開シンポジウム要旨集，p. 43，千葉，2017 年 1 月．

Acknowledgments

This thesis would not have been completed without the help and support of the gentle people around me. I would like to express my deepest gratitude to my supervisor, Professor Satoyuki Kawano, for his support and guidance for my studies throughout the Master's and PhD courses, for his kindness, motivation, and immense knowledge. I would like to thank Associate Professor Kentaro Doi. I received generous support from he, and he gives insightful comments and suggestions. Advice and comments given by Associate Professor Itsuo Hanasaki in Tokyo University of Agriculture and Technology and Assistant Professor Tetsuro Tsuji have been a great help in my research. My gratitude also extended to my dissertation committee members, Professor Kazuyasu Sugiyama and Professor Shigenobu Ogata, for their valuable comments and extensive discussion. I would like to express my gratitude to Dr. Yoichi Kagaya and Ms. Nami Kikushima for their technical support and helpful advice. I also would like to thank our lab secretaries Ms. Makiko Sawada, Ms. Reiko Matsumoto, Ms. Kana Ichino, and Ms. Yuki Hanato for their help to finish my paperwork and warm encouragement. During my time at Kawano laboratory, I have met many friends whose spend the unforgettable lab trip and lab events, for the countless nights we fight for the deadline. In particular, I am grateful to Dr. Satoshi Uehara, Dr. Osman Omran Osman Mosa, Dr. Sawanya Suwannawong, Dr. Weixin Qian, Mr. Hirotaka Iseki, Mr. Daiki Fujiwara, Mr. Michito Matsuoka, Mr. Ryo Nagura, Mr. Shunsuke Fukazawa, Ms. Moino Imoto, Mr. Hiroki Shirai and Mr. Terutaka Noguchi. Last but not least, I would like to thank my parents for their support throughout my life and giving me a chance to chase my dream. This work was supported by Grant-in-Aid for JSPS Research Fellow.